

Document downloaded from:

<http://hdl.handle.net/10251/160599>

This paper must be cited as:

Belda Palazón, B.; Julian, J.; Coego, A.; Wu, Q.; Zhang, X.; Batistic, O.; Alquraishi, SA.... (2019). ABA inhibits myristoylation and induces shuttling of the RGLG1 E3 ligase to promote nuclear degradation of PP2CA. *The Plant Journal*. 98(5):813-825.
<https://doi.org/10.1111/tpj.14274>



The final publication is available at

<https://doi.org/10.1111/tpj.14274>

Copyright Blackwell Publishing

Additional Information

ABA inhibits myristoylation and induces shuttling of the RGLG1 E3 ligase to promote nuclear degradation of PP2CA

Borja Belda-Palazon^{#1}, Jose Julian^{#1}, Alberto Coego^{#1}, Qian Wu^{#2,3}, Xu Zhang^{2,4}, Oliver Batistic⁵, Saleh A. Alquraishi⁶, Joerg Kudla⁵, Chengcai An² and Pedro L. Rodriguez^{*1}

¹Instituto de Biología Molecular y Celular de Plantas, Consejo Superior de Investigaciones Científicas-Universidad Politécnica de Valencia, ES-46022 Valencia, Spain.

²The State Key Laboratory of Protein and Plant Gene research, College of Life Sciences, School of Agriculture Science, Peking University, Beijing, 100871, P. R. China.

³Department of Plant Molecular Biology. Biophore Building, University of Lausanne, 1015 Lausanne, Switzerland

⁴Department of Molecular Biology and Institute of Genetics and Genomics, University of Geneva, 30 quai Ernest-Ansermet, 1211 Geneva, Switzerland

⁵Institut für Biologie und Biotechnologie der Pflanzen, Universität Münster, Schlossplatz 7, 48149 Münster, Germany

⁶Zoology Department, College of Science, King Saud University, Riyadh 11451, Saudi Arabia.

[#]These authors contributed equally to this work and should be considered co-first author.

^{*}Address correspondence to Pedro L. Rodriguez prodriguez@ibmcp.upv.es

Running title: Nuclear shuttling of RGLG1 enhances ABA signaling

Key words: ABA signaling, RGLG1, E3 ligase, PP2C, ubiquitination, myristoylation, shuttling, *Arabidopsis thaliana*

Summary

Hormone- and stress-induced shuttling of signaling or regulatory proteins is an important cellular mechanism to modulate hormone signaling and cope with abiotic stress. Hormone-induced ubiquitination plays a crucial role to determine half-life of key negative regulators of hormone signaling. For ABA signaling, degradation of clade A PP2Cs, such as PP2CA or ABI1, is a complementary mechanism to PYR/PYL/RCAR-mediated inhibition of PP2C activity. ABA promotes the degradation of PP2CA through the RGLG1 E3 ligase, although it is not known how ABA enhances the interaction of RGLG1 with PP2CA given they are predominantly found in plasma membrane and nucleus, respectively. We demonstrate that ABA modifies the subcellular localization of RGLG1 and promotes nuclear interaction with PP2CA. We found RGLG1 is myristoylated *in vivo*, which facilitates its attachment to plasma membrane. ABA inhibits myristoylation of RGLG1 through downregulation of *N-myristoyltransferase1 (NMT1)* and promotes nuclear translocation of RGLG1 in a cycloheximide-insensitive manner. Enhanced nuclear recruitment of the E3 ligase was also promoted by increasing PP2CA protein levels and the formation of RGLG1-receptor-phosphatase complexes. We show that RGLG1^{Gly2Ala}-mutated in the N-terminal myristoylation site- shows constitutive nuclear localization and causes enhanced response to ABA and salt/osmotic stress. RGLG1/5 can interact with certain monomeric ABA receptors, which facilitates the formation of nuclear complexes such as RGLG1-PP2CA-PYL8. In summary, we provide evidence that an E3 ligase can dynamically re-localize in response to both ABA and increased levels of its target, which reveals a mechanism to explain how ABA enhances RGLG1-PP2CA interaction and hence PP2CA degradation.

Introduction

The phytohormone abscisic acid (ABA) regulates seed dormancy, plant growth, leaf senescence and responses to biotic and abiotic stresses (Cutler et al., 2010). The ABA signaling pathway is initiated by ABA perception through PYRABACTIN RESISTANCE1 (PYR1)/PYR1-LIKE (PYL)/REGULATORY COMPONENTS OF ABA RECEPTORS (RCAR) family of proteins (Ma et al., 2009; Park et al., 2009; Santiago et al., 2009a). This is followed by interaction with and inactivation of clade A protein phosphatase type 2Cs (PP2Cs), such as ABA INSENSITIVE 1 (ABI1) and ABI2, HYPERSENSITIVE TO ABA (HAB1) and HAB2, and PROTEIN PHOSPHATASE 2CA/ABA-HYPERSENSITIVE GERMINATION 3 (PP2CA/AHG3), thereby relieving their inhibition on three ABA-activated SNF1-related protein kinases (SnRK2s), i.e. SnRK2.2/D, 2.3/I and 2.6/E/OST1 (Umezawa et al., 2009; Vlad et al., 2009). Structural and biochemical studies have revealed that PP2Cs are necessary ABA co-receptors able to monitor the occupancy of the receptor ABA-binding pocket to achieve nM affinity for ABA binding (Ma et al., 2009; Santiago et al., 2009b; Moreno-Alvero et al., 2017). Degradation of the PP2Cs is a complementary mechanism to PYR/PYL/RCAR-mediated inhibition of PP2C activity (Kong et al., 2015; Wu et al., 2016). Thus, ABA, in addition to biochemical inhibition of the phosphatases, also follows a relief of repression mechanism involving degradation of negative regulators, which has been previously described for several hormones such as auxin, jasmonate, gibberellins and strigolactones (Lumba et al., 2010). For ABA signaling, it has been demonstrated that ABA induces the degradation of existing ABI1 and PP2CA through the PUB12/13 and RGLG1/5 E3 ligases, respectively, and the ubiquitin (Ub) 26S proteasome system. ABA receptors and ABA are strictly required (in the case of PYR1) or enhance (monomeric receptors) PUB13-mediated ABI1 ubiquitination (Kong et al., 2015). ABA receptors were not required for in vitro ubiquitination of PP2CA by RGLG1/5; however, under in vivo conditions ABA enhanced the interaction of RGLG1/5 with PP2CA through an unknown mechanism (Wu et al., 2016).

Currently, at least six *Arabidopsis* PP2Cs, namely ABI1, ABI2, PP2CA/AHG3, AHG1, HAB1 and HAB2, are known to negatively regulate ABA signaling, and also Highly ABA-Induced (HAI) 1-3 phosphatases, although with

less impact in ABA sensitivity and more to regulate particular drought resistance traits (Rubio et al., 2009; Bhaskara 2012; Tischer et al., 2017). PP2CA is a negative regulator of ABA signaling both in seed and vegetative ABA responses, and RGLG1/5 and other E3 ligases regulate PP2CA half-life (Sheen et al., 1998; Kuhn et al., 2006; Yoshida et al., 2006; Rubio et al., 2009; Lee et al., 2009; Wu et al., 2016). RGLG1/5 are RING-type E3 ligases that belong to a five member family (Wu et al., 2016). Sequence alignment has revealed that RGLG1, 2 and 5 belong to a different branch than RGLG3/4 (Zhang et al., 2012). RGLG1 and RGLG2 show functional overlap in K63-linked polyubiquitination in plasma membrane, which is a proteasome-independent function of RGLG1 and RGLG2 (Yin et al., 2007; Romero-Barrios and Vert, 2018). Indeed the *rglg1 rglg2* double mutant shows reduced amounts of Ub-K63 chain-specific signals for PIN2, which affects regulation of PIN2 turnover and root hair phenotype of iron-deficient plants (Yin et al., 2007; Li and Schmidt, 2010; Leitner et al., 2012). However, RGLG2 is functionally unrelated to RGLG1/5 regarding 26S proteasome-linked polyubiquitination of PP2Cs because RGLG2 does not interact with clade A PP2Cs (Wu et al., 2016). RGLGs have variable N-terminal regions, which might lead to functional diversity. Additionally, *RGLG1* and *RGLG2* have different expression profiles in response to different stimuli. For instance, *RGLG1* shows high induction by ABA, cold, osmotic and salt stress. In contrast, *RGLG2* does not respond to abiotic stress in aerial tissue and only in roots to osmotic and salt stress (Wu et al., 2016; Figure S1).

Overexpression of RGLG1, by enhancing degradation of PP2CA and possibly other PP2Cs, enhances drought resistance (Wu et al., 2016). In contrast, RGLG2 negatively regulates drought stress response (Cheng et al., 2012). According to Cheng et al., (2012) it seems that RGLG2 contributes to the degradation of AtERF53, which is a TF that positively regulates drought-responsive genes. Therefore, stress-induced nuclear translocation of RGLG2 contributes to degradation of a positive factor for stress tolerance, possibly as a desensitization mechanism. Different enzymes and signaling proteins shuttle to the nucleus in response to environmental cues or stress, which allows its interaction with the target proteins (Lee et al., 2015; Bigeard and Hirt, 2018). Both RGLG1 and RGLG2 are plasma membrane-associated proteins with a predicted

N-terminal myristoylation site (Yin et al., 2007; Figure S2). Since RGLG1 is localized in plasma membrane to mediate both K63-linked polyubiquitination and endocytic turnover of plasma-membrane transporters but PP2CA is predominantly localized in nucleus and degraded via 26S proteasome (Wu et al., 2016), we hypothesized that ABA treatment might modify the subcellular localization of RGLG1 and promote its interaction with PP2CA. Additionally, we have investigated where takes place the RGLG1-PP2CA interaction, the role of the N-terminal myristoylation site of RGLG1 to determine its subcellular localization and the effect of ABA on the myristoylation of RGLG1.

RESULTS

RGLG1 is myristoylated and localizes at plasma membrane under non-stress conditions

Indirect evidence of RGLG2 myristoylation was obtained through in vitro transcription-translation experiments performed with radiolabeled myristic acid, which was incorporated into the wild type protein but not into the variant with Gly2 replaced by Ala (G2A) (Yin et al., 2007). In order to further investigate the subcellular localization of RGLG1, we generated RGLG1-GFP and the RGLG1^{G2A}-GFP variant that contains a mutation in the predicted N-terminal myristoylation site and delivered them into leaf cells of *Nicotiana benthamiana* by agroinfiltration (Figure 1a). RGLG1-GFP was shown to co-immunoprecipitate with PP2CA when co-expressed in *N. benthamiana* (Wu et al., 2016) and we provide additional evidence it is a functional protein in *Arabidopsis* (Figure S3) Expression of the corresponding fusion proteins was verified by immunoblot analysis using anti-GFP antibodies (Figure 1b). Whereas RGLG1-GFP was localized mostly outside of the nucleus, RGLG1^{G2A}-GFP showed cytosolic and nuclear localization. Nuclear localization of RGLG1^{G2A}-GFP was confirmed by DAPI staining (Figure 1c; Figure S4). In some cells, a weak nuclear staining was also observed for RGLG1-GFP, which was enhanced by ABA-treatment, whereas RGLG1^{G2A}-GFP showed constitutive strong nuclear localization (Figure 1a and c; Figure S4). In order to distinguish whether non-nuclear protein was localized to the plasma membrane or cytosol, we coexpressed RGLG1-GFP or RGLG1^{G2A}-GFP with the plasma membrane marker OPF-TM23 in tobacco leaf

cells. Next, cells were plasmolyzed by a 500 mM NaCl treatment (as described by Schapire et al., 2008) and we found that RGLG1 was localized significantly at the plasma membrane (significant co-localization with OFP-TM23, Rp and Rs>0.4); whereas non-nuclear RGLG1^{G2A}-GFP exhibited cytosolic localization (Figure 1d).

Additionally we generated *Arabidopsis thaliana* transgenic lines that express either RGLG1-GFP or RGLG1^{G2A}-GFP, and verified the expression of the corresponding fusion proteins (Figure 2a; Figure S5). Direct in vivo demonstration of myristoylation has been achieved only in a few proteins, and only recent large-scale proteomic approaches have expanded the confirmed myristoylome (Majeran et al., 2018). We immunoprecipitated RGLG1-GFP or RGLG1^{G2A}-GFP from *Arabidopsis* lines and analyzed these proteins using anti-myristic acid antibody. Immunoblotting assay detected in vivo myristoylated RGLG1, which was abolished by the Gly2Ala mutation (Figure 2a). Interestingly, ABA treatment dramatically reduced myristoylation of RGLG1 (Figure 2b), which could favour shuttling of the protein to nucleus. Indeed, it is known that myristoylated proteins can dynamically relocalize in response to specific signals (Turnbull and Hemsley, 2017; Majeran et al., 2018). We did data mining in public databases and found that *N-myristoyltransferase1* (*At5g57020*, *NMT1*) expression is diminished by ABA-treatment (Figure S6), which might explain the diminished myristoylation of RGLG1 after ABA treatment. Since NMT1 is the central active enzyme that catalyzes myristoylation, these data predict that ABA might enhance the mobilization of different signaling or regulatory proteins of the myristoylome, which is significantly enriched in them (Turnbull and Hemsley, 2017).

RGLG1 shuttles to nucleus after ABA or salt stress treatment

We examined the subcellular localization of RGLG1-GFP in hypocotyl and root cells of *Arabidopsis*, where ABA signaling plays important roles and which allows easily identifying the cell nucleus by bright-field microscopy (Wu et al., 2012; Belda-Palazon et al., 2018). In hypocotyl cells, we found that RGLG1-GFP was localized both in plasma membrane and small vesicles found close or associated to plasma membrane (Figure 3a). This is in agreement with the previously

observed localization of RGLG1 in plasma membrane and its role in K63-linked polyubiquitination (Yin et al., 2007; Romero-Barrios and Vert, 2018). However, upon 50 μ M ABA treatment for 6 h, a pool of RGLG1-GFP was localized in the cell nucleus. To rule out that DAPI staining might affect *per se* the localization of RGLG1-GFP, we also identified directly the nucleus by bright field microscope analysis (Figure 3b). As a result, in differentiated root cells we also found that after ABA treatment a pool of RGLG1-GFP was localized in the cell nucleus (Figure 3b).

In order to obtain additional data for the ABA-induced nuclear localization of RGLG1, we co-expressed RGLG1-GFP in tobacco leaf cells with the nucleolar marker fibrillarin-RFP (abbreviated as Fib-RFP) (Herranz et al., 2012). Fibrillarin is a component of a nucleolar small nuclear ribonucleoprotein (Hornacek et al., 2017) and accordingly, Fib-RFP specifically marked the nucleoli of tobacco leaf cells (Figure 3c). ABA-treatment increased markedly the number of nuclei decorated both by Fib-RFP and RGLG1-GFP (Figure 3d). Demyristoylation enzymes have not been described in plants; therefore it is possible that myristoylated plasma membrane-localized RGLG1 cannot shuttle to nucleus in response to ABA unless RGLG1 is synthesized *de novo*. In order to analyze this possibility, we also performed ABA-treatment in the presence of cycloheximide (CHX) (Figure 3c). Interestingly, we found that CHX treatment did not prevent shuttling of RGLG1 to cell nucleus (Figure 3c and d; Figure S7); therefore *de novo* biosynthesis of RGLG1 is not required and translocation from plasma membrane to nucleus seems to occur in response to ABA. This result suggests that either proteolytic processing of N-myristoylated RGLG1 occurs or alternative mechanisms can deliver surface proteins to nucleus (Burnaevskiy et al., 2015; Chaumet et al., 2015).

Finally, we examined the subcellular localization of RGLG1-GFP and RGLG1^{G2A}-GFP in leaf cells of *Arabidopsis* (Figure S8). The number of nuclei decorated by RGLG1-GFP increased approximately 3 fold after ABA treatment (Figure S8). Additionally, endomembranes decorated with RGLG1-GFP were more visible after ABA-treatment (Figure S8). Indeed, a dynamic behavior of vesicles decorated by RGLG1-GFP could be observed (Movie S1). Compared to the wild type, RGLG1^{G2A}-GFP decorated more nuclei per area under mock

conditions and showed higher nuclear signal intensity (Figure S8). Because *RGLG1* expression is induced by both ABA and abiotic stress (Figure S1), we analyzed whether either salt stress or calcium treatment affect *RGLG1* localization, because abiotic stress simultaneously increases ABA and calcium concentration (Edel and Kudla, 2016). Interestingly, salt stress and the ubiquitous second messenger Ca^{2+} promoted nuclear localization of *RGLG1* (Figure S8). ABA, salt or calcium-treatment did not significantly affect the cellular distribution of *RGLG1*^{G2A}-GFP, in contrast to *RGLG1*-GFP (Figure S8)

We compared ABA sensitivity in germination of independent *Arabidopsis* lines that constitutively express *RGLG1*-GFP or *RGLG1*^{G2A}-GFP (Figure 3e) Constitutive expression of *RGLG1*^{G2A}-GFP, which is strongly localized in nucleus, produced enhanced sensitivity to ABA-mediated inhibition of seed germination compared to *RGLG1*-GFP (Figure 3e, top). Similar results were obtained for salt and osmotic stress-mediated inhibition of seedling establishment (Figure 3e, bottom). Therefore, nuclear localization of *RGLG1* is biologically relevant to mediate stress response presumably by facilitating PP2C degradation. Taken together, these results suggest that ABA and salt stress promote shuttling of *RGLG1* to the nucleus to facilitate ABA signaling, which is restricted under resting conditions by myristoylation-mediated attachment to the plasma membrane.

***RGLG1* interacts with some monomeric ABA receptors and forms ternary PYL8-*RGLG1*-PP2CA complexes in the nucleus**

In vitro *RGLG1/5*-mediated ubiquitination of PP2CA does not require the presence of ABA or ABA receptors (Wu et al., 2016). However, we could not rule out that in vivo receptor-ABA-phosphatase ternary complexes might be better recognized by *RGLG1/5*, for instance by generating additional contact points between the E3 ligase and the receptor/phosphatase co-receptor complex. Therefore, we investigated whether *RGLG1/5* could interact with ABA receptors using the Y2H assay. Interestingly, we found that several monomeric ABA receptors, i.e. PYL4, PYL8, PYL9 and PYL13, interacted with both *RGLG1* and *RGLG5* (Figure 4a). The *RGLG1*^{G2A} version also interacted with PYL4, PYL8 and PYL9 ABA receptors (Figure S9a). Next, we performed in vitro ubiquitination reactions to test whether GST-PYL4 or GST-PYL8 could be ubiquitinated by

RGLG1. Although the E1-E2-E3 ubiquitination cascade was able to ubiquitinate the E3 ligase (anti-FLAG panel), PYL4 and PYL8 were not ubiquitinated by RGLG1 (anti-GST panel) (Figure 4b). Even in the presence of PP2CA, RGLG1 did not ubiquitinate ABA receptors in similar ubiquitination assays (Wu et al., 2016).

We focused additional work on the PYL8-RGLG1 interaction because PYL8 is an efficient inhibitor of PP2CA and is predominantly localized in the nucleus as PP2CA (Antoni et al., 2012 and 2013; Belda-Palazon et al., 2018). To this end, we generated double transgenic lines in *Arabidopsis* co-expressing RGLG1-GFP and either HA-PYL8 or HA-PYR1 (as a putative negative control) and tested by co-immunoprecipitation assays the interaction of RGLG1 with the HA-tagged receptors and endogenous PP2CA, either in mock or ABA-treated plants (Figure 5a). We found that immunoprecipitated RGLG1 formed complexes with PYL8 and PP2CA in ABA-treated plants. Given that PYL8-ABA-PP2CA complexes have been previously identified (Antoni et al., 2013), the most likely explanation is that ternary complexes are formed in the presence of ABA. Lower input of PYL8 and PP2CA is observed in the absence of ABA-treatment because of enhanced ubiquitination of PYL8 (Belda-Palazon et al., 2018) and reduced *PP2CA* transcript levels (Wu et al., 2016). In contrast, PYR1 did not co-immunoprecipitate with RGLG1-GFP and PP2CA (Figure 5a). Therefore, it seems that ABA facilitates the formation of the PYL8-RGLG1-PP2CA complex by up-regulated transcription of *PP2CA* that leads to increased PP2CA levels, stabilization of PYL8 protein levels and high affinity binding of PP2CA to PYL8 (Santiago et al., 2009a; Antoni et al., 2013; Irigoyen et al., 2014; Wu et al., 2016; Belda-Palazon et al., 2018). Indeed, using transient expression in tobacco cells, we demonstrated that increased PP2CA levels lead to enhanced recruitment of RGLG1 in the nucleus (Figures 5b-d). It is well known that transcripts and protein levels of both ABI1 and PP2CA are increased as a negative feedback mechanism to attenuate ABA signaling (Kong et al., 2015; Wu et al., 2016). In the case of PP2CA, we show that the accumulation of the phosphatase will elicit an enhanced recruitment of RGLG1 in the nucleus (Figure 5c), which might prevent excessive accumulation of the phosphatase to facilitate the resetting of ABA signaling.

To further investigate the subcellular localization of the RGLG1 interactions with PYL8 and PP2CA we performed multicolor BiFC through agroinfiltration in tobacco cells to co-express SCFP^N-PYL8, RGLG1-SCFP^C and VENUS^N-PP2CA (Gehl et al., 2009). The PYL8-RGLG1 interaction was visualized through reconstitution of the SCFP (cyan fluorescence), whereas the RGLG1-PP2CA interaction gave rise to SCFP^C-VENUS^N fluorescent protein (Figure 6a; Figure S9b). After ABA-treatment, the multicolor BiFC revealed the formation of PYL8-RGLG1 and PP2CA-RGLG1 complexes that co-localized in the nucleus, which suggests that ternary complexes could be formed. Since ABA/abiotic stress promote shuttling of RGLG1 to nucleus and the formation of receptor-PP2CA complexes (Antoni et al., 2013), the increase of ABA levels facilitates ubiquitination of PP2CA by RGLG1. The interaction of PYL8-RGLG1-PP2CA could be visualized also in membrane complexes associated to the nuclear envelope, which suggests that ubiquitination of PP2CA might occur in specific nuclear territories.

DISCUSSION

In this work we have investigated the mechanism whereby ABA enhances the interaction of RGLG1/5 with PP2CA. The elucidation of this mechanism is physiologically very relevant because regulation of PP2C activity and protein levels is crucial for ABA signaling. We can distinguish at least three steps in the process of ABA signaling: activation of ABA response, desensitization by accumulation of PP2Cs as a negative feedback mechanism and resetting by degradation of PP2Cs. The interaction of E3 ligases with clade A PP2Cs can regulate potentially all these steps, and therefore it is worthy a better understanding of this process. First of all, we discovered that RGLG1 is myristoylated *in vivo* and localizes mostly at plasma membrane under non-stress conditions. Occasional presence in the nucleus of some cells was observed; however, after ABA treatment myristoylation of RGLG1 was reduced by 70% and the number of nuclei decorated by RGLG1 increased from less than 20% to more than 80% (Figure 2b and 3d). In contrast, constitutive presence of RGLG1^{G2A} in the nucleus was observed (Figure 1c and S8). Therefore both inhibition of RGLG1

myristoylation by ABA and cycloheximide-insensitive translocation of RGLG1 facilitate nuclear interaction with PP2CA. It is known that myristoylated proteins can dynamically relocalize in response to specific signals, and hence we show that ABA is another signal that can mobilize myristoylated proteins. Additionally, ABA treatment increases PP2CA transcripts and protein levels as a negative feedback mechanism (Santiago et al., 2009a; Wu et al., 2016). This facilitates the recruitment of the E3 ligase in the nucleus as we have observed that co-expression of RGLG1 with PP2CA increased nuclear localization of RGLG1 to a level close to the observed for the RGLG1^{G2A} mutant. The artificial G2A mutant showed higher nuclear intensity compared to ABA, salt or calcium treatment because it represents an extreme situation where RGLG1 lacks irreversibly the capability to interact with plasma membrane.

Data mining revealed that *NMT1* expression is diminished by ABA-treatment (Figure S6). Indeed, osmotic stress, oxidative stress and drought also diminish expression of *NMT1* (Figure S6), which suggests that enhanced mobilization of myristoylated proteins might be a plant response to cope with different stresses. In *Arabidopsis* there are two NMTs, NMT1 and NMT2, but little is known about demyristoylation enzymes (Boisson et al., 2003). Indeed, to our knowledge, active enzymatic demyristoylation by a specific plant enzyme has not reported yet. However, nearly 1% of the human proteome harbors an N-myristoyl modification and it has been described a bacterial cysteine protease that catalyzes the hydrolysis of N-myristoylated glycine at the amino terminus of host proteins (Burnaevskiy, et al., 2013 and 2015). Given the importance for multiple cellular processes of protein and lipid interactions mediated by N-myristoylation, it is possible that specific plant proteases might catalyze the hydrolysis of N-myristoylated glycine residues as it has been described for the N-myristoylated glycine of ADP-ribosylation factor1 (Burnaevskiy, et al., 2013). Alternatively, other mechanisms could deliver surface proteins to the nucleus, as nuclear envelope-associated endosomes can discharge their contents into the nuclear envelope and therefore transfer cargo from cell surface into the nucleoplasm (Chaumet et al., 2015). Concerning myristoylation enzymes, NMT1 is the central active enzyme and knock out mutants are lethal (Pierre et al., 2007). NMT2 is regarded as a non active enzyme, due to mutations in the active site. Nevertheless, *NMT2*

is not a pseudogene, as either *NMT2* overexpression lines or *nmt2* mutant show developmental defects, although NMT2 is not able to complement *nmt1* mutants (Pierre et al. 2007). Future research could investigate whether, in addition to transcriptional downregulation of *NMT1* by ABA, there is an effect of ABA on the activity of NMT1 or activation of proteolytic processing at N-myristoylated glycine residues.

Taken together with our previous work on RGLG1 (Wu et al., 2016), we have demonstrated that ABA enhances PP2CA degradation by facilitating the interaction of the E3 ligase RGLG1 and its target in the nucleus, which is dependent on several factors (Figure 6b). First, when ABA levels increase after drought stress, more PP2CA is available for interaction because of ABA-induced up-regulation of *PP2CA*. Second, the formation of receptor-ABA-phosphatase complexes induced by ABA will facilitate their recognition by the E3 ligase because RGLG1 can interact with both the ABA receptor and PP2CA (Figure 6b). Finally, shuttling to nucleus of RGLG1 induced by ABA/abiotic stress allows its interaction with nuclear PP2CA. Therefore the ABA- and receptor-dependent biochemical inhibition of PP2CA also facilitates its ubiquitination and degradation in the nucleus. Inhibition of nuclear PP2C activity allows SnRK2-dependent phosphorylation of several targets, which leads to inhibition of the SWI/SNF chromatin remodelling ATPase BRAHMA -a repressor of ABA signaling- and activation of ABRE-binding factors (Peirats-Llobet et al., 2016, Lynch et al., 2012). Conversely, nuclear accumulation of phosphatase can block ABA signaling as described for *abi1*^{Gly180Asp} (Moes et al., 2008). In summary, we show that hormone- and stress-induced shuttling of an E3 ligase is an important cellular mechanism to regulate hormonal signaling and cope with abiotic stress. Additionally, a better understanding of the dynamic RGLG1-PP2CA interaction is provided in this work.

EXPERIMENTAL PROCEDURES

Plant material and generation of transgenic plants

Arabidopsis thaliana plants were grown as described by Pizzio et al., (2013). Constructs of RGLG1-GFP and RGLG1^{Gly2Ala}-GFP driven by 35S promoter in

pBIN121 were generated as described in Wu et al., (2016). To introduce RGLG1^{Gly2Ala} mutation, PCR was performed to replace the second Gly to Ala in RGLG1 cDNA using QuikChange Lightning Multi Site-Directed Mutagenesis Kit (Agilent Technologies). The pBIN121 35S:*RGLG1-GFP* and *RGLG1^{Gly2Ala}-GFP* constructs were transferred to *Agrobacterium tumefaciens* pGV2260 by electroporation and used to transform Col-0 plants by the floral dipping method (Clough and Bent, 1998). Seeds of transformed plants were harvested and plated on kanamycin (50 µg/ml) selection medium to identify T1 transgenic plants and T3 progenies homozygous for the selection marker were used for further studies. To generate RGLG1-GFP×HA-PP2CA, RGLG1-GFP×HA-PYL8 and RGLG1-GFP×HA-PYR1 double transgenic plants, *Arabidopsis* plants carrying RGLG1-GFP were transformed with pAlligator2 constructs encoding HA-tagged PP2CA, PYL8 or PYR1, respectively. Seeds of transformed plants were selected by analysis of GFP fluorescence in the seed and sowed in soil to obtain the T2 generation. Homozygous T3 progeny was used for further studies and expression of HA-tagged protein was verified by immunoblot analysis using anti-HA-HRP. We also generated a second group of pMDC83 35S:*RGLG1-GFP* and *RGLG1^{Gly2Ala}-GFP* constructs and the corresponding transgenic plants for phenotype analysis (Curtis and Grossniklaus, 2003). In this case, seeds of plants transformed with pMDC83 constructs were selected on hygromycin (20 µg/ml) supplemented medium and T3 progenies homozygous for the selection marker were used for further studies.

Transient protein expression in *Nicotiana benthamiana*

Agrobacterium infiltration of tobacco leaves was performed basically as described by Saez et al., (2008). To investigate the subcellular localization of RGLG1-GFP, RGLG1^{Gly2Ala}-GFP and PP2CA-GFP we used the pBIN121 and pMDC83 vectors, which express the proteins driven by the 35S promoter (Curtis and Grossniklaus, 2003; Antoni et al., 2012). To generate RGLG1-RFP, we used the gateway pGWB554 vector, which contains the attR1 and attR2 recombination sites in front of mRFP1 (Nakagawa et al., 2007). When indicated, *A. tumefaciens* cultures containing constructs that express either RGLG1-RFP or PP2CA-GFP were co-infiltrated at different ratios in tobacco leaves. To perform multicolor BiFC we cloned RGLG1 into p(MAS)-SCYCE, PYL8 into pDEST-SCYNE(R) and

PP2CA into pDEST-VYNE(R) vectors, as described by Gehl et al., (2009). The different binary vectors were introduced into *Agrobacterium tumefaciens* C58C1 (pGV2260) by electroporation and transformed cells were selected in LB plates supplemented with kanamycin (50 µg/ml). Then, they were grown in liquid LB medium to late exponential phase and cells were harvested by centrifugation and resuspended in 10 mM morpholinoethanesulphonic (MES) acid-KOH pH 5.6 containing 10 mM MgCl₂ and 150 mM acetosyringone to an OD_{600 nm} of 1. These cells were mixed with an equal volume of *Agrobacterium* C58C1 (pCH32 35S:p19) expressing the silencing suppressor p19 of tomato bushy stunt virus so that the final density of *Agrobacterium* solution was about 1. Bacteria were incubated for 3 h at room temperature and then injected into young fully expanded leaves of 4-week-old *Nicotiana benthamiana* plants. Leaves were examined 48–72 h after infiltration using confocal laser scanning microscopy. The plasma membrane GFP-TM23 and nucleolar fibrillarin-RFP markers have been described previously (Herranz et al., 2012; Rodriguez et al., 2014).

Yeast two hybrid (Y2H) assay

To test the interaction among PYR/PYL ABA receptors and RGLG1/5, full length cDNAs of 12 ABA receptors were cloned from an *Arabidopsis* cDNA library and then cloned into pGADT7. The interaction assay was performed as described in Wu et al., (2016). Additionally, wild-type RGLG1 and RGLG1^{Gly2Ala} were cloned into pGADT7 and tested with pGBKT7-PYL4, pGBKT7-PYL8 and pGBKT7-PYL9.

In vitro ubiquitination assay

For in vitro substrate ubiquitination assay, a total reaction volume of 30 µl was mixed by adding 500 ng purified MBP-RGLG1, 300 ng GST-PYL4 or GST-PYL8, 50 ng E1 (Sigma), 100 ng E2 UbcH5b (Enzo Life Sciences), 3 µg FLAG-tagged ubiquitin (Sigma), 10 mM phosphocreatine, and 0.1 unit of creatine kinase in the ubiquitination buffer (50 mM Tris-HCl pH 7.5, 3 mM ATP, 5 mM MgCl₂, and 0.5 mM DTT) and incubated at 37 °C for 2 h. The reaction was stopped by adding 4× SDS loading buffer. Samples were separated by 8% SDS-PAGE gel and analyzed by western blot using anti-GST (Abmart), anti-FLAG (Sigma) or anti-MBP (Earthox) antibody.

Protein extraction, analysis, immunodetection and colP

Protein extracts for immunodetection experiments were prepared from the single or double *Arabidopsis* transgenic lines described above. Material (~100 mg) for direct Western blot analysis was extracted in 2X Laemmli buffer (125 mM Tris-HCl pH 6.8, 4% SDS, 20% glycerol, 2% mercaptoethanol, 0.001% bromophenol blue), proteins were run in a 4-15% SDS-PAGE MiniProtean precast gel (BioRad) and analyzed by immunoblotting. Proteins were transferred onto Immobilon-P membranes (Millipore) and probed with anti-HA-peroxidase (Roche; 1:2000 dilution) or anti-GFP monoclonal antibody (clone JL-8; Clontech; 1:10000 dilution) as primary antibody and ECL anti-mouse peroxidase (GE Healthcare; 1:5000 dilution) as secondary antibody. Detection was performed using the ECL select western blotting detection kit (GE Healthcare). Image capture was done using the image analyzer LAS3000 and quantification of the protein signal was done using Image Guache V4.0 software.

Protein extracts for co-IP experiments were prepared from *Arabidopsis* transgenic lines. Samples were collected, ground in liquid nitrogen and immediately placed in 50 mM Tris-HCl pH 8.0, 150 mM NaCl, 1% Triton X-100, 3mM DTT, 50 μ M MG-132 and protease inhibitor cocktail on ice for protein extraction. Homogenates were cleared by centrifugation at 12000 g, 4°C for 15 min, and supernatants were used for immunoprecipitation. RGLG1-GFP was immunoprecipitated using super-paramagnetic micro MACS beads coupled to monoclonal anti-GFP antibody according to the manufacturer's instructions (Miltenyi Biotec). Purified immunocomplexes were eluted in Laemmli buffer, boiled and run in a 10% SDS-PAGE gel. Proteins immunoprecipitated with anti-GFP antibody were transferred onto Immobilon-P membranes (Millipore) and probed with anti-HA-peroxidase or anti-PP2CA (Wu et al., 2016) to detect colP of HA-tagged PYR1/PYL8 or endogenous PP2CA proteins, respectively.

Confocal Laser Scanning Microscopy (CLSM)

Confocal imaging was performed using a Zeiss LSM 780 AxioObserver.Z1 laser scanning microscope with C-Apochromat 40x/1.20 W corrective water immersion objective. The following fluorophores, which were excited and fluorescence emission detected by frame switching in the single or multi-tracking mode at the indicated wavelengths, were used in tobacco leaf infiltration experiments: GFP

(488 nm/500-530 nm), YFP (488 nm/529-550 nm), OFP (561 nm/575-600 nm), SCFP 405 nm/450-485 nm and RFP (561 nm/605-630 nm). Pinholes were adjusted to 1 Air Unit for each wavelength. Post-acquisition image processing was performed using ZEN (ZEISS Efficient Navigation) Lite 2012 imaging software and ImageJ (<http://rsb.info.gov/ij/>).

Seed germination and seedling establishment assays

After surface sterilization of the seeds, stratification was conducted in the dark at 4°C for 3 d. Approximately 100 seeds of each genotype were sowed on MS plates lacking or supplemented with 0.5 μ M ABA, 50 mM NaCl or 200 mM mannitol. To score seed germination, radical emergence was analyzed at 48-72 h after sowing. Seedling establishment was scored as the percentage of seeds that developed green expanded cotyledons at 96 h.

Statistics and colocalization analyses

Student's T-test was performed for single comparisons. Values are averages obtained from three independent experiments \pm SD. Fluorescence colocalization analysis was performed using PSC colocalization plug-in of ImageJ (French et al., 2008). Pearson's (Rp) and Spearman's (Rs) correlation coefficients in the range 0.4-1 indicate co-localization, whereas lower values indicate lack of co-localization.

In vivo myristoylation assay

RGLG1-GFP or RGLG1^{Gly2Ala}-GFP were immunoprecipitated using super-paramagnetic micro MACS beads coupled to monoclonal anti-GFP antibody according to the manufacturer's instructions (Miltenyi Biotec). Immunoprecipitated proteins were analyzed by SDS-PAGE and immunoblotting. To detect the myristoylation of RGLG1-GFP, the immunoprecipitated protein was probed with anti-myristic acid antibody (ab37027, 1:1.000) followed by secondary anti-rat antibody (1:10.000, Thermo Scientific A18739). Detection was performed using the SuperSignal West Femto luminescence kit (Thermo Scientific).

Nuclei staining and counting

The reagent 4, 6-diamidino-2-phenylindole (DAPI;Sigma,St.Louis,MO) was used for staining nuclei. For the CLSM analysis hypocotyl/root cells of *Arabidopsis* seedlings or agro-infiltrated *N. benthamiana* leaves were stained with 1 mL of 5 µg/ml DAPI solution and were analyzed using a Zeiss LSM 780 AxioObserver.Z1 laser scanning microscope with C-Apochromat 403/1.20-W corrective water immersion objective. Fluorescence was detected using the following excitation/emission parameters: 405nm/440-540 nm and 488 nm/495-530 nm for DAPI and GFP channels, respectively. Post-acquisition image processing was performed using ZEN (ZEISS Efficient Navigation) Lite 2012 imaging software and ImageJ v1.8 (<https://imagej.nih.gov/ij/>). Leaf sections were mounted on a microscope slide and covered with distilled water for observation through the leaf abaxial side. Nuclei counting was done in sections of 40000 µm² (n=20 fields) from 5 independent plants, analyzed through a full z-series of confocal images.

ACKNOWLEDGEMENTS

Work in P.L.R.'s laboratory was supported by the Ministerio de Ciencia e Innovacion, Fondo Europeo de Desarrollo Regional and Consejo Superior de Investigaciones Cientificas through grants BIO2014-52537-R and BIO2017-82503-R. This work was also funded by grants from the Deutsche Forschungsgemeinschaft (DFG) Ku931/4-1 to J.K., and BA4742/1-2 to O.B. B.B. was funded by Programa VALi+d GVA APOSTD/2017/039. J.J. was supported by a FPI contract from MINECO.

The authors declare no conflicts of interest.

SUPPORTING INFORMATION

Additional Supporting Information may be found in the online version of this article.

Figure S1. *RGLG1* expression is strongly up-regulated by ABA and cold, in contrast to *RGLG2*.

Figure S2. Scheme of the RGLG1 protein.

Figure S3. RGLG1-GFP is a functional protein and ABA enhances its interaction with PP2CA.

Figure S4. DAPI staining reveals constitutive nuclear localization of RGLG1^{G2A}-GFP.

Figure S5. Immunoblot analysis confirms the expression of RGLG1-GFP and G2A-GFP proteins in *Arabidopsis* overexpressing lines.

Figure S6. Expression of *NMT1* is down-regulated by ABA.

Figure S7. CHX treatment does not prevent ABA-induced shuttling of RGLG1 to cell nucleus in tobacco leaf cells.

Figure S8. ABA, salt and calcium promote shuttling of RGLG1 to nucleus.

Figure S9. Interactions between RGLG1^{G2A} and PYLs in Y2H assay.

Movie S1. Dynamic behavior of vesicles decorated by RGLG1-GFP.

REFERENCES

- Antoni, R., Gonzalez-Guzman, M., Rodriguez, L., Rodrigues, A., Pizzio, G. A., and Rodriguez, P. L.** (2012). Selective Inhibition of Clade A Phosphatases Type 2C by PYR/PYL/RCAR Abscisic Acid Receptors. *Plant Physiol.* **158**, 970-980.
- Antoni, R., Gonzalez-Guzman, M., Rodriguez, L., Peirats-Llobet, M., Pizzio, G. A., Fernandez, M. A., De Winne, N., De Jaeger, G., Dietrich, D., Bennett, M. J., and Rodriguez, P. L.** (2013). PYRABACTIN RESISTANCE1-LIKE8 plays an important role for the regulation of abscisic acid signaling in root. *Plant Physiol.* **161**, 931-941.
- Belda-Palazon, B., Gonzalez-Garcia, M. P., Lozano-Juste, J., Coego, A., Antoni, R., Julian, J., Peirats-Llobet, M., Rodriguez, L., Berbel, A., Dietrich, D., Fernandez, M. A., Madueno, F., Bennett, M. J., and Rodriguez, P. L.** (2018). PYL8 mediates ABA perception in the root through non-cell-autonomous and ligand-stabilization-based mechanisms. *Proc. Natl. Acad. Sci. USA* **15**, E11857-E11863.
- Bhaskara, G. B., Nguyen, T. T., and Verslues, P. E.** (2012). Unique drought resistance functions of the highly ABA-induced clade A protein phosphatase 2Cs. *Plant Physiol.* **160**, 379-395.
- Bigeard, J. and Hirt, H.** (2018). Nuclear Signaling of Plant MAPKs. *Front Plant Sci.* **9**, 469.
- Boisson, B., Giglione, C., and Meinel, T.** (2003). Unexpected protein families including cell defense components feature in the N-myristoylome of a higher eukaryote. *J. Biol. Chem.* **278**, 43418-43429.
- Burnaevskiy, N., Peng, T., Reddick, L. E., Hang, H. C., and Alto, N. M.** (2015). Myristoylome profiling reveals a concerted mechanism of ARF GTPase deacylation by the bacterial protease IpaJ. *Mol. Cell* **58**, 110-122.
- Burnaevskiy, N., Fox, T. G., Plymire, D. A., Ertelt, J. M., Weigele, B. A., Selyunin, A. S., Way, S. S., Patrie, S. M., and Alto, N. M.** (2013). Proteolytic elimination of N-myristoyl modifications by the Shigella virulence factor IpaJ. *Nature* **496**, 106-109.
- Chaumet, A., Wright, G. D., Seet, S. H., Tham, K. M., Gounko, N. V., and Bard, F.** (2015). Nuclear envelope-associated endosomes deliver surface proteins to the nucleus. *Nat. Commun.* **6**, 8218.
- Cheng, M. C., Hsieh, E. J., Chen, J. H., Chen, H. Y., and Lin, T. P.** (2012). Arabidopsis RGLG2, functioning as a RING E3 ligase, interacts with AtERF53 and negatively regulates the plant drought stress response. *Plant Physiol.* **158**, 363-375.
- Clough, S. J. and Bent, A. F.** (1998). Floral dip: a simplified method for Agrobacterium-mediated transformation of Arabidopsis thaliana. *Plant J.* **16**, 735-743.
- Curtis, M. D. and Grossniklaus, U.** (2003). A gateway cloning vector set for high-throughput functional analysis of genes in planta. *Plant Physiol.* **133**, 462-469.
- Cutler, S. R., Rodriguez, P. L., Finkelstein, R. R., and Abrams, S. R.** (2010). Abscisic acid: emergence of a core signaling network. *Annu. Rev. Plant Biol.* **61**, 651-679.
- Edel, K. H. and Kudla, J.** (2016). Integration of calcium and ABA signaling. *Curr. Opin. Plant Biol.* **33**, 83-91.
- French, A. P., Mills, S., Swarup, R., Bennett, M. J., and Pridmore, T. P.** (2008). Colocalization of fluorescent markers in confocal microscope images of plant cells. *Nat. Protoc.* **3**, 619-628.
- Gehl, C., Waadt, R., Kudla, J., Mendel, R. R., and Hansch, R.** (2009). New GATEWAY vectors for high throughput analyses of protein-protein interactions by bimolecular fluorescence complementation. *Mol. Plant* **2**, 1051-1058.
- Herranz, M. C., Pallas, V., and Aparicio, F.** (2012). Multifunctional roles for the N-terminal basic motif of Alfalfa mosaic virus coat protein: nucleolar/cytoplasmic shuttling, modulation of RNA-binding activity, and virion formation. *Mol. Plant Microbe Interact.* **25**, 1093-1103.
- Hornacek, M., Kovacik, L., Mazel, T., Cmarko, D., Bartova, E., Raska, I., and Smirnov, E.** (2017). Fluctuations of pol I and fibrillarin contents of the nucleoli. *Nucleus* **8**, 421-432.
- Irigoyen, M. L., Iniesto, E., Rodriguez, L., Puga, M. I., Yanagawa, Y., Pick, E., Strickland, E., Paz-Ares, J., Wei, N., De Jaeger, G., Rodriguez, P. L., Deng, X. W., and Rubio, V.** (2014). Targeted degradation of abscisic acid receptors is mediated by the ubiquitin ligase substrate adaptor DDA1 in Arabidopsis. *Plant Cell* **26**, 712-728.
- Kong, L., Cheng, J., Zhu, Y., Ding, Y., Meng, J., Chen, Z., Xie, Q., Guo, Y., Li, J., Yang, S., and Gong, Z.** (2015). Degradation of the ABA co-receptor ABI1 by PUB12/13 U-box E3 ligases. *Nat. Commun.* **6**, 8630.
- Kuhn, J. M., Boisson-Dernier, A., Dizon, M. B., Maktabi, M. H., and Schroeder, J. I.** (2006). The protein phosphatase AtPP2CA negatively regulates abscisic acid signal transduction in Arabidopsis, and effects of abh1 on AtPP2CA mRNA. *Plant Physiol.* **140**, 127-139.

- Lee, S. C., Lan, W., Buchanan, B. B., and Luan, S. (2009). A protein kinase-phosphatase pair interacts with an ion channel to regulate ABA signaling in plant guard cells. *Proc. Natl. Acad. Sci. USA* **106**, 21419-21424.
- Lee, H. J., Park, Y. J., Seo, P. J., Kim, J. H., Sim, H. J., Kim, S. G., and Park, C. M. (2015). Systemic Immunity Requires SnRK2.8-Mediated Nuclear Import of NPR1 in Arabidopsis. *Plant Cell* **27**, 3425-3438.
- Leitner, J., Petrusek, J., Tomanov, K., Retzer, K., Parezova, M., Korbei, B., Bachmair, A., Zazimalova, E., and Luschnig, C. (2012). Lysine63-linked ubiquitylation of PIN2 auxin carrier protein governs hormonally controlled adaptation of Arabidopsis root growth. *Proc. Natl. Acad. Sci. USA* **109**, 8322-8327.
- Li, W. and Schmidt, W. (2010). A lysine-63-linked ubiquitin chain-forming conjugase, UBC13, promotes the developmental responses to iron deficiency in Arabidopsis roots. *Plant J.* **62**, 330-343.
- Lynch, T., Erickson, B. J., and Finkelstein, R. R. (2012). Direct interactions of ABA-insensitive(ABI)-clade protein phosphatase(PP)2Cs with calcium-dependent protein kinases and ABA response element-binding bZIPs may contribute to turning off ABA response. *Plant Mol. Biol.* **80**, 647-658.
- Lumba, S., Cutler, S., and McCourt, P. (2010). Plant nuclear hormone receptors: a role for small molecules in protein-protein interactions. *Annu. Rev. Cell Dev. Biol.* **26**, 445-469.
- Ma, Y., Szostkiewicz, I., Korte, A., Moes, D., Yang, Y., Christmann, A., and Grill, E. (2009). Regulators of PP2C Phosphatase Activity Function as Abscisic Acid Sensors. *Science* **324**, 1064-1068.
- Majeran, W., Le Caer, J. P., Ponnala, L., Meinel, T., and Giglione, C. (2018). Targeted profiling of *A. thaliana* sub-proteomes illuminates new co- and post-translationally N-terminal Myristoylated proteins. *Plant Cell* **30**, 543-562.
- Moes, D., Himmelbach, A., Korte, A., Haberer, G., and Grill, E. (2008). Nuclear localization of the mutant protein phosphatase *abi1* is required for insensitivity towards ABA responses in Arabidopsis. *Plant J.* **54**, 806-819.
- Moreno-Alvero, M., Yunta, C., Gonzalez-Guzman, M., Lozano-Juste, J., Benavente, J. L., Arbona, V., Menendez, M., Martinez-Ripoll, M., Infantes, L., Gomez-Cadenas, A., Rodriguez, P. L., and Albert, A. (2017). Structure of Ligand-Bound Intermediates of Crop ABA Receptors Highlights PP2C as Necessary ABA Co-receptor. *Mol. Plant* **10**, 1250-1253.
- Nakagawa, T., Suzuki, T., Murata, S., Nakamura, S., Hino, T., Maeo, K., Tabata, R., Kawai, T., Tanaka, K., Niwa, Y., Watanabe, Y., Nakamura, K., Kimura, T., and Ishiguro, S. (2007). Improved Gateway binary vectors: high-performance vectors for creation of fusion constructs in transgenic analysis of plants. *Biosci. Biotechnol. Biochem.* **71**, 2095-2100.
- Park, S. Y., Fung, P., Nishimura, N., Jensen, D. R., Fujii, H., Zhao, Y., Lumba, S., Santiago, J., Rodrigues, A., Chow, T. F. F., Alfred, S. E., Bonetta, D., Finkelstein, R., Provar, N. J., Desveaux, D., Rodriguez, P. L., McCourt, P., Zhu, J. K., Schroeder, J. I., Volkman, B. F., and Cutler, S. R. (2009). Abscisic Acid Inhibits Type 2C Protein Phosphatases via the PYR/PYL Family of START Proteins. *Science* **324**, 1068-1071.
- Peirats-Llobet, M., Han, S. K., Gonzalez-Guzman, M., Jeong, C. W., Rodriguez, L., Belda-Palazon, B., Wagner, D., and Rodriguez, P. L. (2016). A Direct Link between Abscisic Acid Sensing and the Chromatin-Remodeling ATPase BRAHMA via Core ABA Signaling Pathway Components. *Mol. Plant* **9**, 136-147.
- Pierre, M., Traverso, J. A., Boisson, B., Domenichini, S., Bouchez, D., Giglione, C., and Meinel, T. (2007). N-myristoylation regulates the SnRK1 pathway in Arabidopsis. *Plant Cell* **19**, 2804-2821.
- Rodriguez, L., Gonzalez-Guzman, M., Diaz, M., Rodrigues, A., Izquierdo-Garcia, A. C., Peirats-Llobet, M., Fernandez, M. A., Antoni, R., Fernandez, D., Marquez, J. A., Mulet, J. M., Albert, A., and Rodriguez, P. L. (2014). C2-Domain Abscisic Acid-Related Proteins Mediate the Interaction of PYR/PYL/RCAR Abscisic Acid Receptors with the Plasma Membrane and Regulate Abscisic Acid Sensitivity in Arabidopsis. *Plant Cell* **26**, 4802-4820.
- Romero-Barríos, N. and Vert, G. (2018). Proteasome-independent functions of lysine-63 polyubiquitination in plants. *New Phytol.* **217**, 995-1011.
- Rubio, S., Rodrigues, A., Saez, A., Dizon, M. B., Galle, A., Kim, T. H., Santiago, J., Flexas, J., Schroeder, J. I., and Rodriguez, P. L. (2009). Triple loss of function of protein phosphatases type 2C leads to partial constitutive response to endogenous abscisic acid. *Plant Physiol.* **150**, 1345-1355.

- Saez, A., Rodrigues, A., Santiago, J., Rubio, S., and Rodriguez, P. L.** (2008). HAB1-SWI3B interaction reveals a link between abscisic acid signaling and putative SWI/SNF chromatin-remodeling complexes in Arabidopsis. *Plant Cell* **20**, 2972-2988.
- Santiago, J., Rodrigues, A., Saez, A., Rubio, S., Antoni, R., Dupeux, F., Park, S. Y., Marquez, J. A., Cutler, S. R., and Rodriguez, P. L.** (2009a). Modulation of drought resistance by the abscisic acid receptor PYL5 through inhibition of clade A PP2Cs. *Plant J.* **60**, 575-588.
- Santiago, J., Dupeux, F., Round, A., Antoni, R., Park, S. Y., Jamin, M., Cutler, S. R., Rodriguez, P. L., and Marquez, J. A.** (2009b). The abscisic acid receptor PYR1 in complex with abscisic acid. *Nature* **462**, 665-668.
- Schapiro, A. L., Voigt, B., Jasik, J., Rosado, A., Lopez-Cobollo, R., Menzel, D., Salinas, J., Mancuso, S., Valpuesta, V., Baluska, F., and Botella, M. A.** (2008). Arabidopsis synaptotagmin 1 is required for the maintenance of plasma membrane integrity and cell viability. *Plant Cell* **20**, 3374-3388.
- Sheen, J.** (1998). Mutational analysis of protein phosphatase 2C involved in abscisic acid signal transduction in higher plants. *Proc. Natl. Acad. Sci. USA* **95**, 975-980.
- Tischer, S. V., Wunschel, C., Papacek, M., Kleigewe, K., Hofmann, T., Christmann, A., and Grill, E.** (2017). Combinatorial interaction network of abscisic acid receptors and coreceptors from Arabidopsis thaliana. *Proc. Natl. Acad. Sci. USA* **114**, 10280-10285.
- Turnbull, D. and Hemsley, P. A.** (2017). Fats and function: protein lipid modifications in plant cell signalling. *Curr. Opin. Plant Biol.* **40**, 63-70.
- Umezawa, T., Sugiyama, N., Mizoguchi, M., Hayashi, S., Myouga, F., Yamaguchi-Shinozaki, K., Ishihama, Y., Hirayama, T., and Shinozaki, K.** (2009). Type 2C protein phosphatases directly regulate abscisic acid-activated protein kinases in Arabidopsis. *Proc. Natl. Acad. Sci. USA* **106**, 17588-17593.
- Vlad, F., Rubio, S., Rodrigues, A., Sirichandra, C., Belin, C., Robert, N., Leung, J., Rodriguez, P. L., Lauriere, C., and Merlot, S.** (2009). Protein phosphatases 2C regulate the activation of the Snf1-related kinase OST1 by abscisic acid in Arabidopsis. *Plant Cell* **21**, 3170-3184.
- Wu, C., Feng, J., Wang, R., Liu, H., Yang, H., Rodriguez, P. L., Qin, H., Liu, X., and Wang, D.** (2012). HRS1 acts as a negative regulator of abscisic acid signaling to promote timely germination of Arabidopsis seeds. *PLoS. One* **7**, e35764.
- Wu, Q., Zhang, X., Peirats-Llobet, M., Belda-Palazon, B., Wang, X., Cui, S., Yu, X., Rodriguez, P. L., and An, C.** (2016). Ubiquitin Ligases RGLG1 and RGLG5 Regulate Abscisic Acid Signaling by Controlling the Turnover of Phosphatase PP2CA. *Plant Cell* **28**, 2178-2196.
- Yin, X. J., Volk, S., Ljung, K., Mehlmer, N., Dolezal, K., Ditengou, F., Hanano, S., Davis, S. J., Schmelzer, E., Sandberg, G., Teige, M., Palme, K., Pickart, C., and Bachmair, A.** (2007). Ubiquitin lysine 63 chain forming ligases regulate apical dominance in Arabidopsis. *Plant Cell* **19**, 1898-1911.
- Yoshida, T., Nishimura, N., Kitahata, N., Kuromori, T., Ito, T., Asami, T., Shinozaki, K., and Hirayama, T.** (2006). ABA-hypersensitive germination3 encodes a protein phosphatase 2C (AtPP2CA) that strongly regulates abscisic acid signaling during germination among Arabidopsis protein phosphatase 2Cs. *Plant Physiol.* **140**, 115-126.
- Zhang, X., Wu, Q., Ren, J., Qian, W., He, S., Huang, K., Yu, X., Gao, Y., Huang, P., and An, C.** (2012). Two novel RING-type ubiquitin ligases, RGLG3 and RGLG4, are essential for jasmonate-mediated responses in Arabidopsis. *Plant Physiol.* **160**, 808-822.

FIGURE LEGENDS

Figure 1. Subcellular localization of RGLG1 depends on the N-terminal myristoylation site.

(a) Nuclear accumulation of RGLG1 is restricted by the N-terminal myristoylation site. The photographs show the subcellular localization of RGLG1-GFP or RGLG1^{G2A}-GFP expressed in epidermal leaf cells of *Nicotiana benthamiana* using pBIN121. Scale bars = 30 μ m. (b) Expression of RGLG1-GFP and G2A-GFP in *Nicotiana benthamiana*. Anti-GFP immunoblotting analysis was performed to verify the expression of the corresponding fusion proteins. Ponceau staining of rubisco was used as a protein loading control. (c) DAPI staining reveals nuclear localization of RGLG1^{G2A}-GFP. The photographs show the subcellular localization of RGLG1^{G2A}-GFP expressed in epidermal cells of *Nicotiana benthamiana*. Arrows indicate the cell nucleus. Scale bars = 10 μ m. (d) RGLG1 is preferentially localized at the plasma membrane, whereas the G2A mutant is found in the cytosol. After transient expression in *N. benthamiana*, the cells were plasmolyzed using a 500 mM NaCl treatment for 30 min. Confocal images show transiently transformed tobacco epidermal cells co-expressing either RGLG1-GFP or RGLG1^{G2A}-GFP and the plasma membrane marker OFP-TM23. The degree of colocalization between the two fluorescent signals was analyzed using merged images and Zen Lite software and measuring values of Pearson's (Rp) and Spearman's (Rs) correlation coefficients (French et al., 2008).

Figure 2. ABA inhibits myristoylation of RGLG1.

(a) In vivo myristoylation of RGLG1-GFP. RGLG1-GFP or RGLG1^{G2A}-GFP were expressed in *Arabidopsis* transgenic lines, immunoprecipitated from *Arabidopsis* protein extracts and immunoblotted using anti-GFP or anti-myristic acid antibodies. (b) ABA treatment (50 μ M for 6 h) reduces myristoylation of RGLG1. Analysis of RGLG1-GFP myristoylation was performed as described in (a) and the signal obtained after immunoblotting was quantified using Image J (relative value=1 in the absence of ABA). Values are averages obtained from three independent experiments. Data are averages of three independent experiments.

Figure 3. ABA promotes shuttling of RGLG1 to cell nucleus.

(a, b) Nuclear localization of RGLG1 in *Arabidopsis* hypocotyl cells (a) or root cells (b) was promoted by 50 μ M ABA treatment for 6 h. The photographs show the subcellular localization of RGLG1-GFP expressed in hypocotyl (a) or root cells (b) of *Arabidopsis* transgenic lines using pMDC83. The GFP channel shows the subcellular localization of RGLG1-GFP; Bright field (BF) microscope imaging served to identify nuclei, which was confirmed by DAPI staining. Nuclei are indicated by arrows. Scale bars=10 μ m. (c) CHX treatment does not prevent ABA-induced shuttling of RGLG1 to cell nucleus in tobacco leaf cells. The photographs show the subcellular localization of RGLG1-GFP expressed in epidermal leaf cells of *N. benthamiana* that were mock-, 50 μ M ABA-treated or simultaneously ABA- and CHX-treated for 6 h. De novo biosynthesis of RGLG1 was inhibited by 100 μ M CHX treatment. The GFP channel shows the subcellular localization of RGLG1-GFP, whereas the RFP channel shows the localization of the nucleolar marker Fib-RFP. CHX treatment led to simultaneous staining of nucleolus and nucleoplasm by Fib-RFP. The intensity profiles of GFP (green) and RFP (red) fluorescence were measured along the indicated distance (microns) of the selected yellow boxes. (d) Percentage of nuclei decorated only by Fib-RFP or simultaneously by Fib-RFP + RGLG1-GFP. * indicates $P < 0.05$ (Student's t test) compared to mock-treated samples. (e) Constitutive expression of RGLG1^{G2A}-GFP leads to enhanced sensitivity to 0.5 μ M ABA-mediated inhibition of germination (left) or 50 mM NaCl and 200 mM mannitol-mediated inhibition of seedling establishment (right) compared to RGLG1-GFP. * indicates $P < 0.05$ (Student's t test) compared to the average of RGLG1-GFP in the same assay conditions. Germination was scored 3 d after sowing seeds of two independent lines generated with pMDC83-35S (top panel), whereas establishment - percentage of seeds that developed green expanded cotyledons- was scored 4 d after sowing seeds of two independent lines generated with pBIN121-35S (bottom panel).

Figure 4. Interactions between RGLG1/5 and PYR/PYLs in Y2H assay.

(a) Full-length PYR/PYLs were used as preys in pGAD vectors and RGLG1/5 as baits in pGBD vectors, respectively. Dilutions of saturated yeast cultures were

spotted onto the plates and photographs were taken after 5 days. Yeast Nitrogen Base (YNB) medium –LT lacks Leu and Trp, whereas medium –LTHA lacks Leu, Trp, His and Ade. (b) MBP-RGLG1 (E3) does not ubiquitinate in vitro the PYL4 or PYL8 receptors (anti-GST panel). In contrast, in vitro autoubiquitination of MBP-RGLG1 (anti-FLAG panel) was observed when the E1-E2-E3 components were combined. FLAG-Ub was used to detect the incorporation of Ub into the E1-E2-E3 cascade.

Figure 5. Immunoprecipitation of RGLG1 pulls-down PYL8 and PP2CA in ABA-treated plants.

(a) Co-immunoprecipitation experiments suggest the formation of RGLG1 complexes with PP2CA and PYL8 after 50 μ M ABA-treatment in *Arabidopsis* double transgenic lines co-expressing RGLG1-GFP and HA-PYL8. Endogenous PP2CA was detected using the E2663 anti-PP2CA antibody (Wu et al., 2016). In contrast, PYR1 does not form such complexes in *Arabidopsis* double transgenic lines co-expressing RGLG1-GFP and HA-PYR1. (b) Nuclear localization of RGLG1 is increased after co-expression with PP2CA. The photographs show the subcellular localization of RGLG1-RFP expressed by agroinfiltration in epidermal *N. benthamiana* cells in the absence or presence of PP2CA-GFP at different ratios, which reflect the relative concentration of agrobacteria used in the different co-infiltrations, ranging from 1:0 to 1:1 (RGLG1-RFP:PP2CA-GFP). Asterisks are close to nuclei. Scale bars = 20 μ m. (c) Histograms indicate the relative number of nuclei decorated by RGLG1-RFP per area (40000 μ m², n=20 fields from 5 independent plants). (d) Immunoblotting analysis using α -RFP or α -GFP was used to verify the expression of the corresponding fusion proteins.

Figure 6. Model to explain how ABA enhances the interaction of RGLG1 with PP2CA.

(a) Multicolor BiFC reveals the formation of PYL8-RGLG1 and PP2CA-RGLG1 complexes that co-localize in the nucleus of tobacco leaves after ABA treatment. Confocal images of transiently transformed tobacco epidermal cells co-expressing SCFP^N-PYL8, RGLG1-SCFP^C and VENUS^N-PP2CA. The PYL8-RGLG1 interaction was visualized through reconstitution of the SCFP, whereas

the RGLG1-PP2CA interaction gave rise to SCFP^C-VENUS^N fluorescent protein. The interacting proteins could be visualized in the nucleus and membrane complexes associated to the nuclear envelope. To perform multicolor BiFC, RGLG1 was cloned into p(MAS)-SCYCE, PYL8 into pDEST-SCYNE(R) and PP2CA into pDEST-VYNE(R) vectors, as described by Gehl et al., (2009). Constructs were delivered into tobacco leaves through *Agrobacterium*-mediated transfection. Leaves were examined using CLSM 48-72 h after infiltration in the absence of exogenous ABA or previous 50 mM ABA-treatment for 1 h. Scale bars = 30 or 40 μm for minus or plus exogenous ABA treatment, respectively. (b) Proposed model for the enhanced degradation of PP2CA mediated by ABA, PYL8 and RGLG1. Under non-stress conditions (top, low ABA levels), RGLG1 shows less interaction with PP2CA (dashed arrow) because more protein is attached to plasma membrane via N-myristoylated Glycine 2 (purple circle). Other unidentified E3s might regulate PP2CA levels. PP2CA interacts with SnRK2s, which prevents their activation and leads to the inhibition of downstream ABA responses. PP2Cs themselves also inhibit downstream targets such as TFs and SLAC1. When plants are submitted to abiotic stress (bottom, high ABA levels), ABA promotes the interaction of certain PYLs with PP2CA, inhibiting its phosphatase activity. Additionally ABA promotes inhibition of RGLG1 myristoylation and cycloheximide-insensitive translocation to nucleus (NE, nuclear envelope), where receptor-ABA-PP2CA complexes are formed. RGLG1 recognition of PP2CA is facilitated in the receptor-ABA-PP2CA complex.

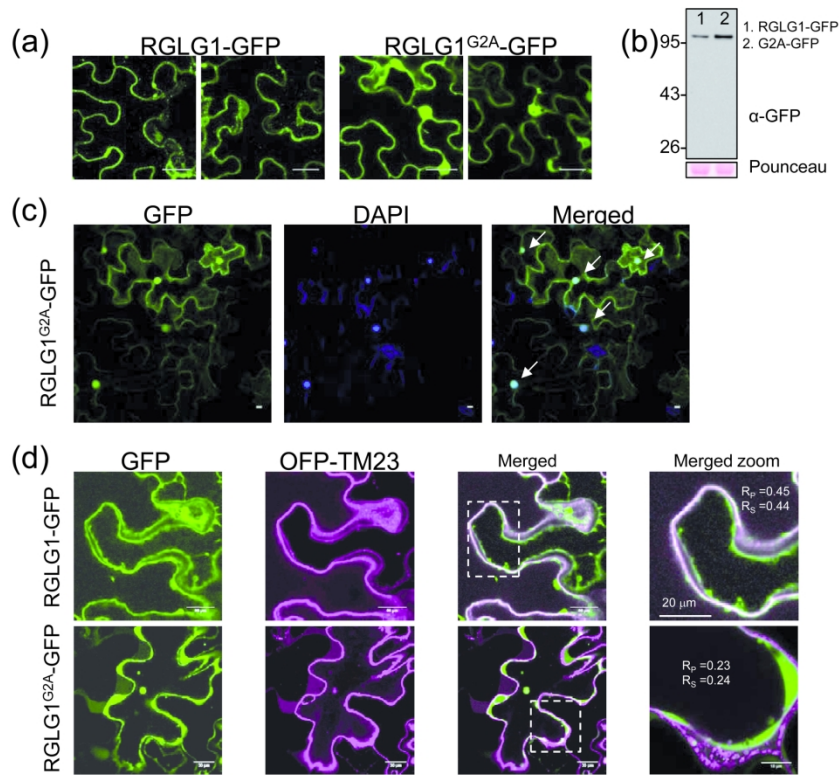


Figure 1. Subcellular localization of RGLG1 depends on the N-terminal myristoylation site.

(a) Nuclear accumulation of RGLG1 is restricted by the N-terminal myristoylation site. The photographs show the subcellular localization of RGLG1-GFP or RGLG1^{G2A}-GFP expressed in epidermal leaf cells of *Nicotiana benthamiana* using pBIN121. Scale bars = 30 μ m. (b) Expression of RGLG1-GFP and G2A-GFP in *Nicotiana benthamiana*. Anti-GFP immunoblotting analysis was performed to verify the expression of the corresponding fusion proteins. Ponceau staining of rubisco was used as a protein loading control. (c) DAPI staining reveals nuclear localization of RGLG1^{G2A}-GFP. The photographs show the subcellular localization of RGLG1^{G2A}-GFP expressed in epidermal cells of *Nicotiana benthamiana*. Arrows indicate the cell nucleus. The GFP channel shows the subcellular localization of RGLG1^{G2A}-GFP, whereas the DAPI channel shows mostly the nuclei (indicated by arrows in the merged panel). Scale bars = 10 μ m. (d) RGLG1 is preferentially localized at the plasma membrane, whereas the G2A mutant is found in the cytosol. After transient expression in *N. benthamiana*, the cells were plasmolyzed using a 500 mM NaCl treatment for 30 min. Confocal images show transiently transformed tobacco epidermal cells co-expressing either RGLG1-GFP or RGLG1^{G2A}-GFP and the plasma membrane marker OFF-TM23. The degree of colocalization between the two fluorescent signals was analyzed using merged images and Zen Lite software and measuring values of Pearson's (R_p) and Spearman's (R_s) correlation coefficients (French et al., 2008).

Figure 1

183x242mm (300 x 300 DPI)

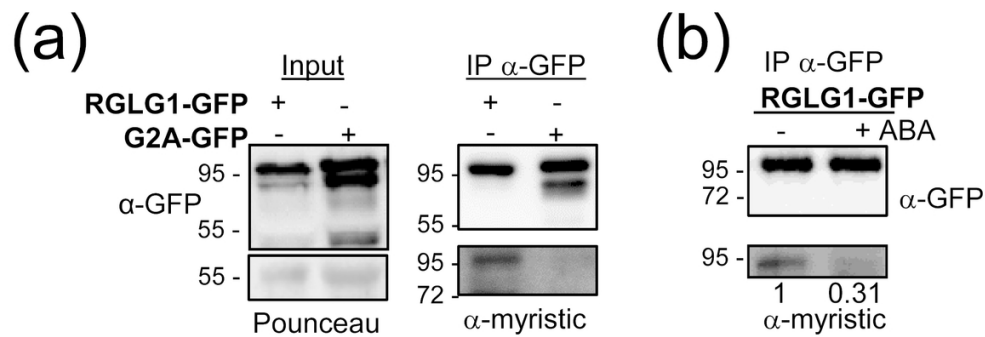


Figure 2. ABA inhibits myristoylation of RGLG1.

(a) In vivo myristoylation of RGLG1-GFP. RGLG1-GFP or RGLG1^{G2A}-GFP were expressed in *Arabidopsis* transgenic lines, immunoprecipitated from *Arabidopsis* protein extracts and immunoblotted using anti-GFP or anti-myristic acid antibodies. (b) ABA treatment (50 μ M for 6 h) reduces myristoylation of RGLG1. Analysis of RGLG1-GFP myristoylation was performed as described in (a) and the signal obtained after immunoblotting was quantified using Image J (relative value=1 in the absence of ABA). Data are averages of three independent experiments.

Figure 2

99x112mm (300 x 300 DPI)

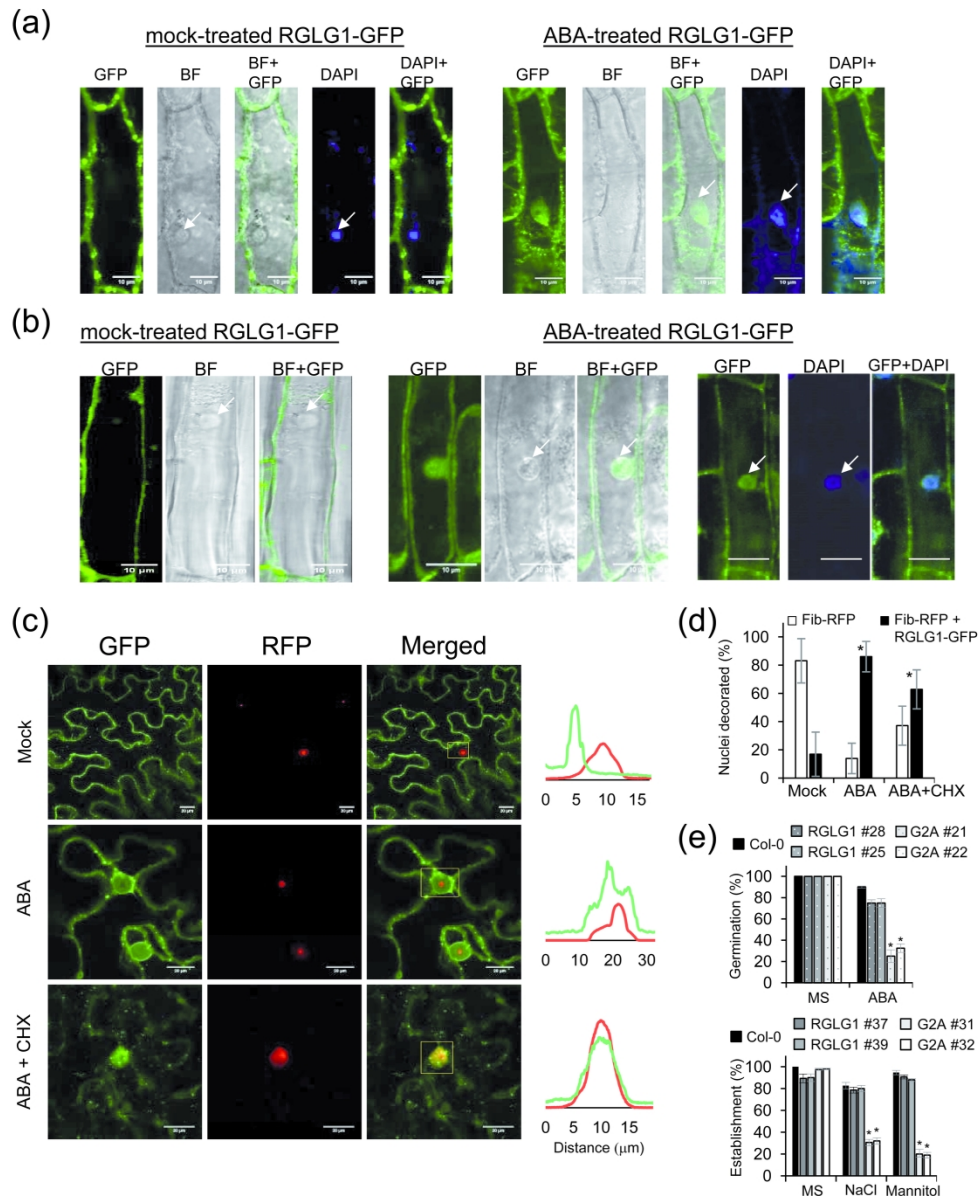


Figure 3. ABA induces shuttling of RGLG1 to cell nucleus. (a, b) Nuclear localization of RGLG1 in Arabidopsis hypocotyl cells (a) or root cells (b) was promoted by 50 μ M ABA treatment for 6 h. The photographs show the subcellular localization of RGLG1-GFP expressed in hypocotyl (a) or root cells (b) of Arabidopsis transgenic lines using pMDC83. The GFP channel shows the subcellular localization of RGLG1-GFP; Bright field (BF) microscope imaging served to identify nuclei, which was confirmed by DAPI staining. Nuclei are indicated by arrows. Scale bars=10 μ m. (c) CHX treatment does not prevent ABA-induced shuttling of RGLG1 to cell nucleus in tobacco leaf cells. The photographs show the subcellular localization of RGLG1-GFP expressed in epidermal leaf cells of *N. benthamiana* that were mock-, 50 μ M ABA-treated or simultaneously ABA- and CHX-treated for 6 h. De novo biosynthesis of RGLG1 was inhibited by 100 μ M CHX treatment. The GFP channel shows the subcellular localization of RGLG1-GFP, whereas the RFP channel shows the localization of the nucleolar marker Fib-RFP. CHX treatment led to simultaneous staining of nucleolus and nucleoplasm by Fib-RFP. The intensity profiles of GFP (green) and RFP (red) fluorescence were measured along the indicated distance (microns) of the selected yellow boxes. (d) Percentage of nuclei decorated only by Fib-RFP or simultaneously by Fib-RFP + RGLG1-GFP. * indicates $P < 0.05$ (Student's t test)

compared to mock-treated samples. (e) Constitutive expression of RGLG1G2A-GFP leads to enhanced sensitivity to 0.5 μ M ABA-mediated inhibition of germination (top) or 50 mM NaCl and 200 mM mannitol-mediated inhibition of seedling establishment (bottom) compared to RGLG1-GFP. * indicates $P < 0.05$ (Student's t test) compared to the average of RGLG1-GFP in the same assay conditions. Germination was scored 3 d after sowing seeds of two independent lines generated with pMDC83-35S (top panel), whereas establishment -percentage of seeds that developed green expanded cotyledons- was scored 4 d after sowing seeds of two independent lines generated with pBIN121-35S (bottom panel).

190x232mm (300 x 300 DPI)

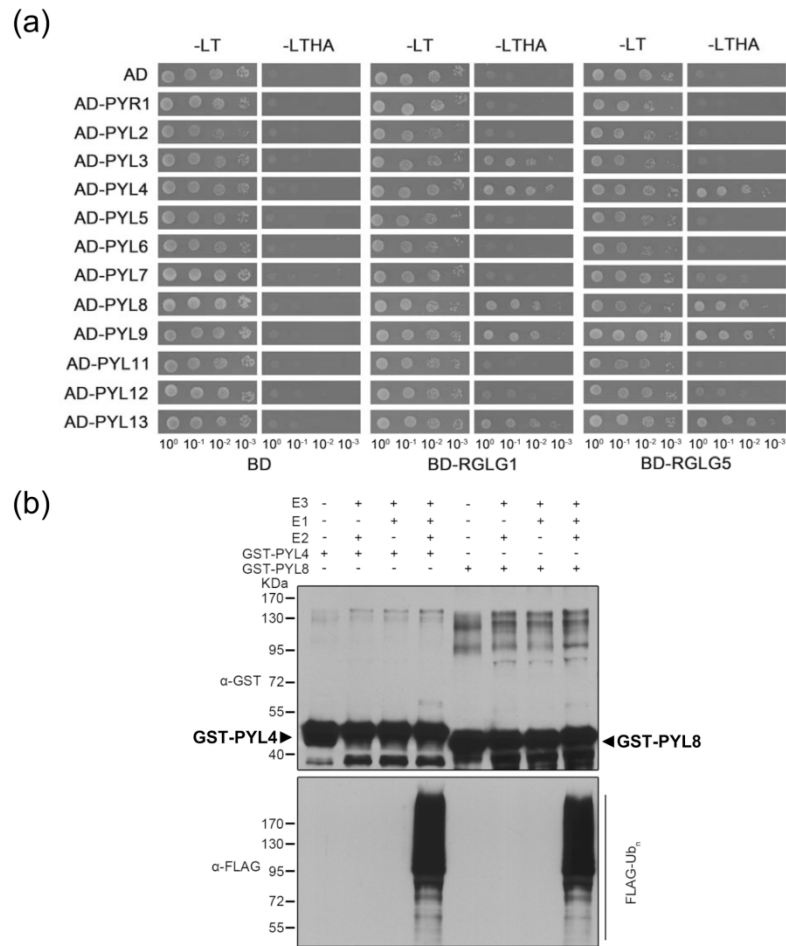


Figure 4. Interactions between RGLG1/5 and PYR/PYLs in Y2H assay.

(a) Full-length PYR/PYLs were used as preys in pGAD vectors and RGLG1/5 as baits in pGBD vectors, respectively. Dilutions of saturated yeast cultures were spotted onto the plates and photographs were taken after 5 days. Yeast Nitrogen Base (YNB) medium -LT lacks Leu and Trp, whereas medium -LTHA lacks Leu, Trp, His and Ade. (b) MBP-RGLG1 (E3) does not ubiquitinate *in vitro* the PYL4 or PYL8 receptors (anti-GST panel). In contrast, *in vitro* autoubiquitination of MBP-RGLG1 (anti-FLAG panel) was observed when the E1-E2-E3 components were combined. FLAG-Ub was used to detect the incorporation of Ub into the E1-E2-E3 cascade.

Figure 4

172x243mm (300 x 300 DPI)

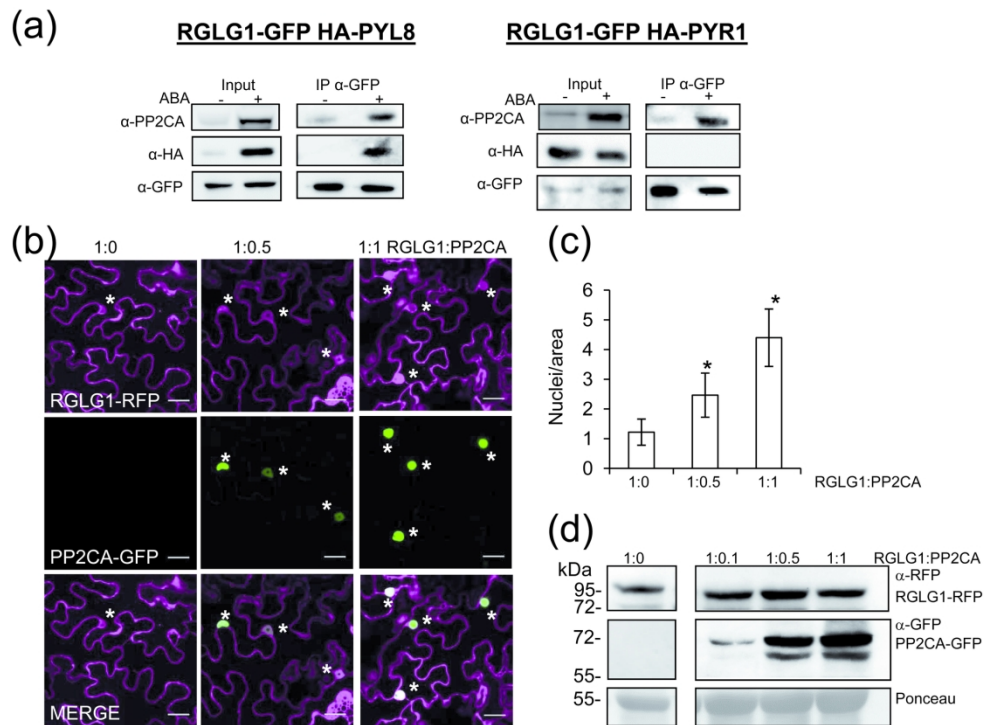


Figure 5. Immunoprecipitation of RGLG1 pulls-down PYL8 and PP2CA in ABA-treated plants.

(a) Co-immunoprecipitation experiments suggest the formation of RGLG1 complexes with PP2CA and PYL8 after 50 μ M ABA-treatment in *Arabidopsis* double transgenic lines co-expressing RGLG1-GFP and HA-PYL8. Endogenous PP2CA was detected using the E2663 anti-PP2CA antibody (Wu et al., 2016). In contrast, PYR1 does not form such complexes in *Arabidopsis* double transgenic lines co-expressing RGLG1-GFP and HA-PYR1. (b) Nuclear localization of RGLG1 is increased after co-expression with PP2CA. The photographs show the subcellular localization of RGLG1-RFP expressed by agroinfiltration in epidermal *N. benthamiana* cells in the absence or presence of PP2CA-GFP at different ratios, which reflect the relative concentration of agrobacteria used in the different co-infiltrations, ranging from 1:0 to 1:1 (RGLG1-RFP:PP2CA-GFP). Asterisks are close to nuclei. Scale bars = 20 μ m (c) Histograms indicate the relative number of nuclei decorated by RGLG1-RFP per area (40000 μ m², n=20 fields from 5 independent plants). (d) Immunoblotting analysis using α -RFP or α -GFP was used to verify the expression of the corresponding fusion proteins.

Figure 5

183x217mm (300 x 300 DPI)

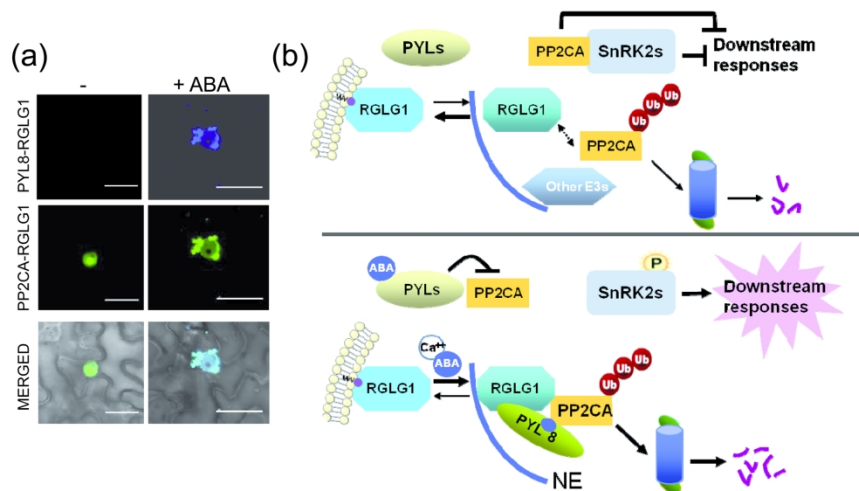


Figure 6. Model to explain how ABA enhances the interaction of RGLG1 with PP2CA.

(a) Multicolor BiFC reveals the formation of PYL8-RGLG1 and PP2CA-RGLG1 complexes that co-localize in the nucleus of tobacco leaves after ABA treatment. Confocal images of transiently transformed tobacco epidermal cells co-expressing SCFP^N-PYL8, RGLG1-SCFP^C and VENUS^N-PP2CA. The PYL8-RGLG1 interaction was visualized through reconstitution of the SCFP, whereas the RGLG1-PP2CA interaction gave rise to SCFP^C-VENUS^N fluorescent protein. The interacting proteins could be visualized in the nucleus and membrane complexes associated to the nuclear envelope. To perform multicolor BiFC, RGLG1 was cloned into p(MAS)-SCYCE, PYL8 into pDEST-SCYNE(R) and PP2CA into pDEST-VYNE(R) vectors, as described by Gehl et al., (2009). Constructs were delivered into tobacco leaves through Agrobacterium-mediated transfection. Leaves were examined using CLSM 48-72 h after infiltration in the absence of exogenous ABA or previous 50 μ M ABA-treatment for 1 h. Scale bars = 30 or 40 μ m for minus or plus exogenous ABA treatment, respectively. (b) Proposed model for the enhanced degradation of PP2CA mediated by ABA, PYL8 and RGLG1. Under non-stress conditions (top, low ABA levels), RGLG1 shows less interaction with PP2CA (dashed arrow) because more protein is attached to plasma membrane via N-myristoylated Glycine 2 (purple circle). Other unidentified E3s might regulate PP2CA levels. PP2CA interacts with SnRK2s, which prevents their activation and leads to the inhibition of downstream ABA responses. PP2Cs themselves also inhibit downstream targets such as TFs and SLAC1. When plants are submitted to abiotic stress (bottom, high ABA levels), ABA promotes the interaction of certain PYLs with PP2CA, inhibiting its phosphatase activity. Additionally ABA promotes inhibition of RGLG1 myristoylation and cycloheximide-insensitive translocation to nucleus (NE, nuclear envelope), where receptor-ABA-PP2CA complexes are formed. RGLG1 recognition of PP2CA is facilitated in the receptor-ABA-PP2CA complex.

Figure 6

183x248mm (300 x 300 DPI)

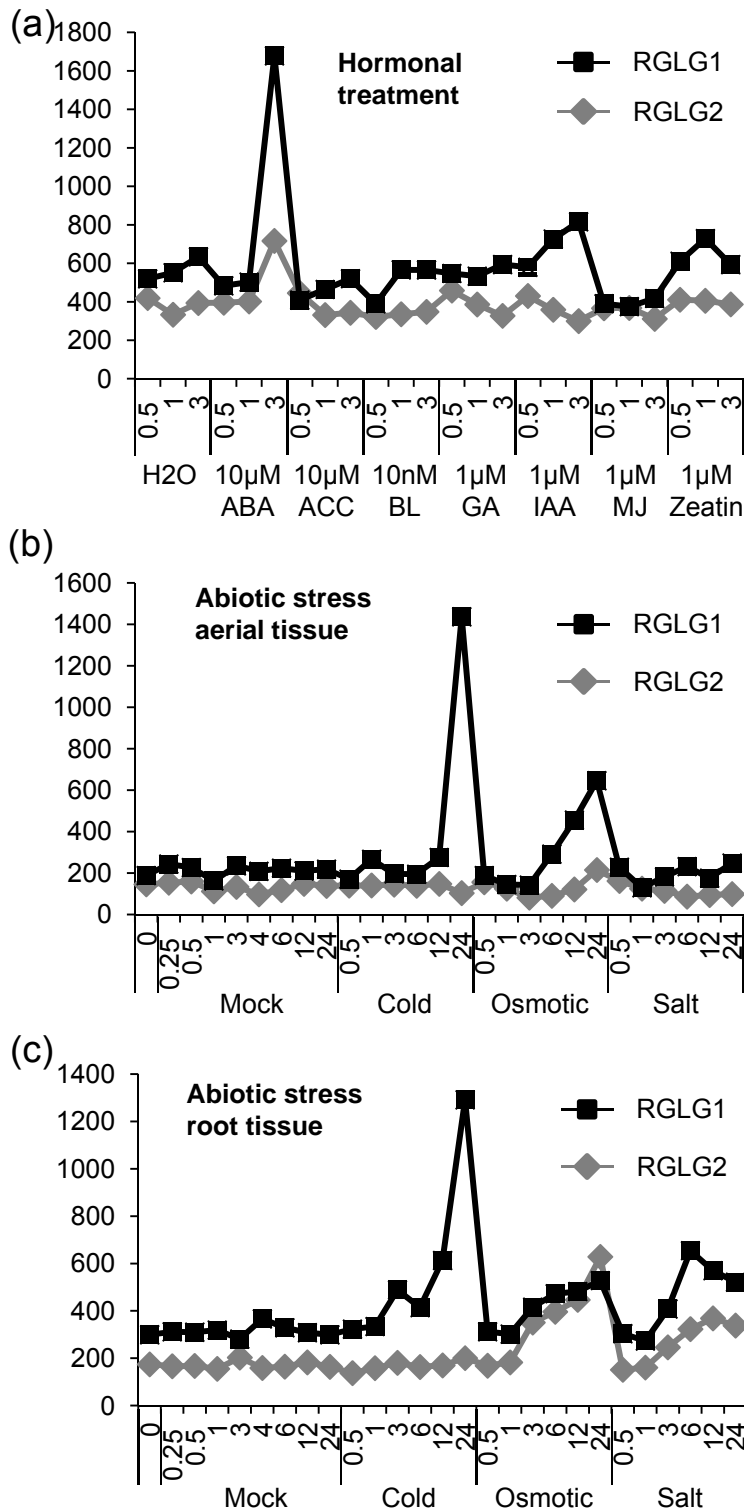


Figure S1. *RGLG1* expression is strongly upregulated by ABA and cold, in contrast to *RGLG2*.

Relative expression of *RGLG1* and *RGLG2* in seedlings that were treated with different hormones (a) or submitted to cold (4°C), osmotic (300 mM mannitol) or salt (150 mM NaCl) stress (b, c). Expression data were obtained from Affymetrix microarrays for *Arabidopsis* deposited in AtGenExpress public database (Goda et al., 2008) and visualized using the AtGenExpress Visualization Tool located in <http://weigelworld.org/resources.html>.



Intrinsic disorder profile

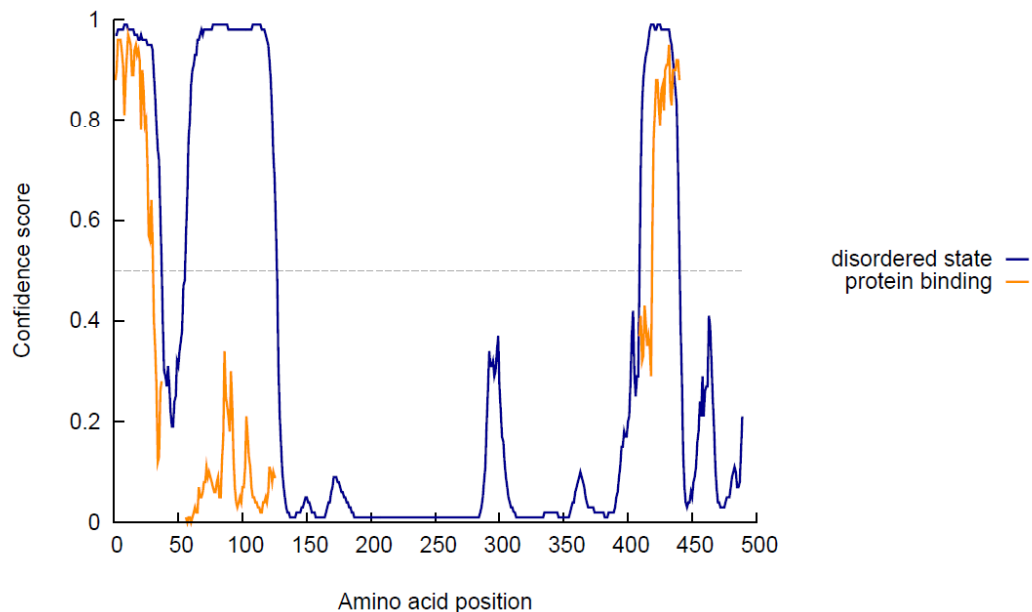


Figure S2. Scheme of the RGLG1 protein.

The position of the N-terminal myristoylation site, secondary structure prediction (pink, α -helix; yellow, β -sheet), the intrinsic disorder profile (bottom) and the RING finger (conserved Cys and His residues labeled by asterisks) are indicated. Analysis was performed using PSIPRED and DISOPRED3 prediction servers (<http://bioinf.cs.ucl.ac.uk>). The graph (bottom) shows the DISOPRED3 disorder confidence levels against the sequence positions as a solid blue line. The grey dashed horizontal line marks the threshold above which amino acids are regarded as disordered. For disordered residues, the orange line shows the confidence of disordered residues being involved in protein-protein interactions, i.e. the disordered region folds upon binding to an interacting protein.

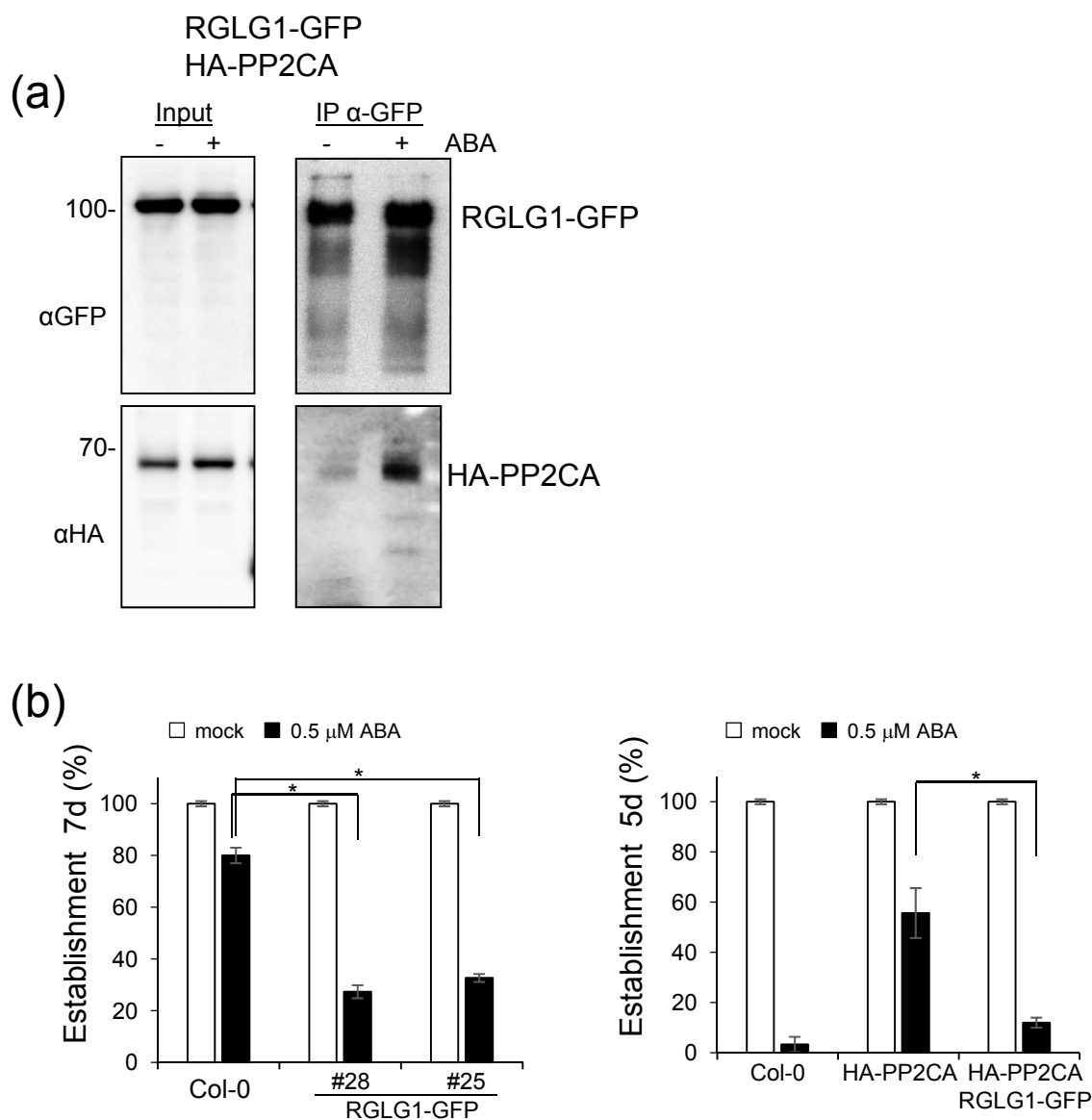


Figure S3. RGLG1-GFP is a functional protein and ABA enhances its interaction with PP2CA.

(a) Co-immunoprecipitation experiments reveal the interaction of RGLG1-GFP with HA-PP2CA, which was markedly enhanced after 50 μM ABA-treatment for 6 h. Experiments were conducted in two week-old *Arabidopsis* transgenic plants co-expressing both RGLG1-GFP and HA-PP2CA. (b) Overexpression of RGLG1-GFP confers enhanced sensitivity to ABA-mediated inhibition of seedling establishment (left) and abolishes the ABA-insensitive phenotype generated by overexpression of HA-PP2CA (right). Seedling establishment was scored 7 d after sowing for RGLG1-GFP lines (left panel) and 5 d after sowing for lines expressing either HA-PP2CA or co-expressing both RGLG1-GFP and HA-PP2CA (right panel). * indicates $P < 0.05$ (Student's t test) when the lines expressing RGLG1-GFP were compared to Col-0 (left) or co-expression of RGLG1-GFP + HA-PP2CA was compared to HA-PP2CA line (right) in the same assay conditions.

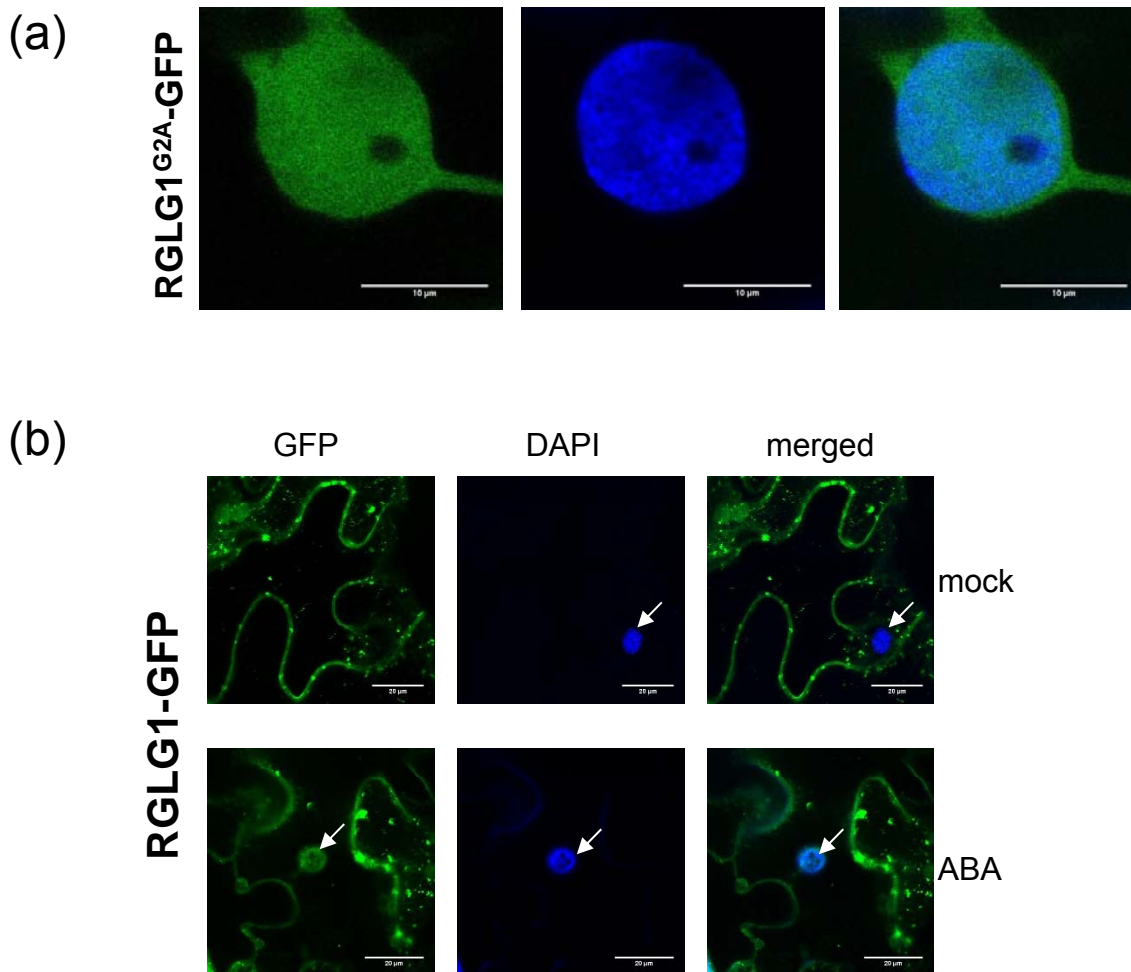


Figure S4. DAPI staining reveals constitutive nuclear localization of RGLG1^{G2A}-GFP.

(a) Nuclei of tobacco leaves were stained with 5 $\mu\text{g/ml}$ DAPI at 72 h after agroinfiltration with a construct encoding RGLG1^{G2A}-GFP. Approximately 1 mL of the DAPI solution was infiltrated and leaves were analyzed immediately using a Zeiss LSM 780 AxioObserver.Z1 laser scanning microscope with C-Apochromat 403/1.20-W corrective water immersion objective. Fluorescence was detected using the following excitation/emission parameters: 405 nm/440-540 nm and 488 nm/495-530 nm for DAPI and GFP channels, respectively. Post-acquisition image processing was performed using ZEN (ZEISS Efficient Navigation) Lite 2012 imaging software and ImageJ v1.8 (<https://imagej.nih.gov/ij/>). Scale bars = 10 μm . (b) ABA-treatment promotes shuttling of RGLG1 to cell nucleus. The photographs show the subcellular localization of RGLG1-GFP expressed in epidermal leaf cells of *N. benthamiana*. Tobacco leaves were incubated 48 h post-agroinfiltration with a mock or 50 μM ABA solution for 6 h and subsequently stained with DAPI solution. Arrows indicate the cell nucleus. Scale bars = 20 μm .

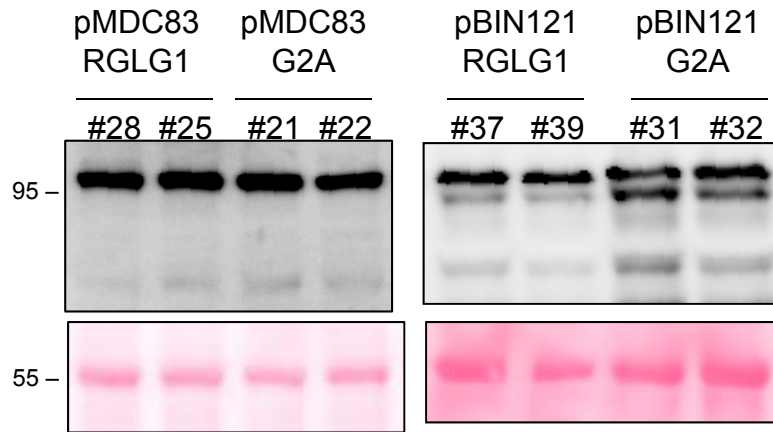


Figure S5. Immunoblot analysis confirms the expression of RGLG1-GFP and G2A-GFP proteins in *Arabidopsis* overexpressing lines.

Protein extracts were prepared from pMDC83-based or pBIN121-based transgenic lines, extracted in 2X Laemmli buffer, run in a 4-10% SDS-PAGE gel and analyzed by immunoblotting using anti-GFP antibodies. Ponceau staining shows Rubisco protein loading.

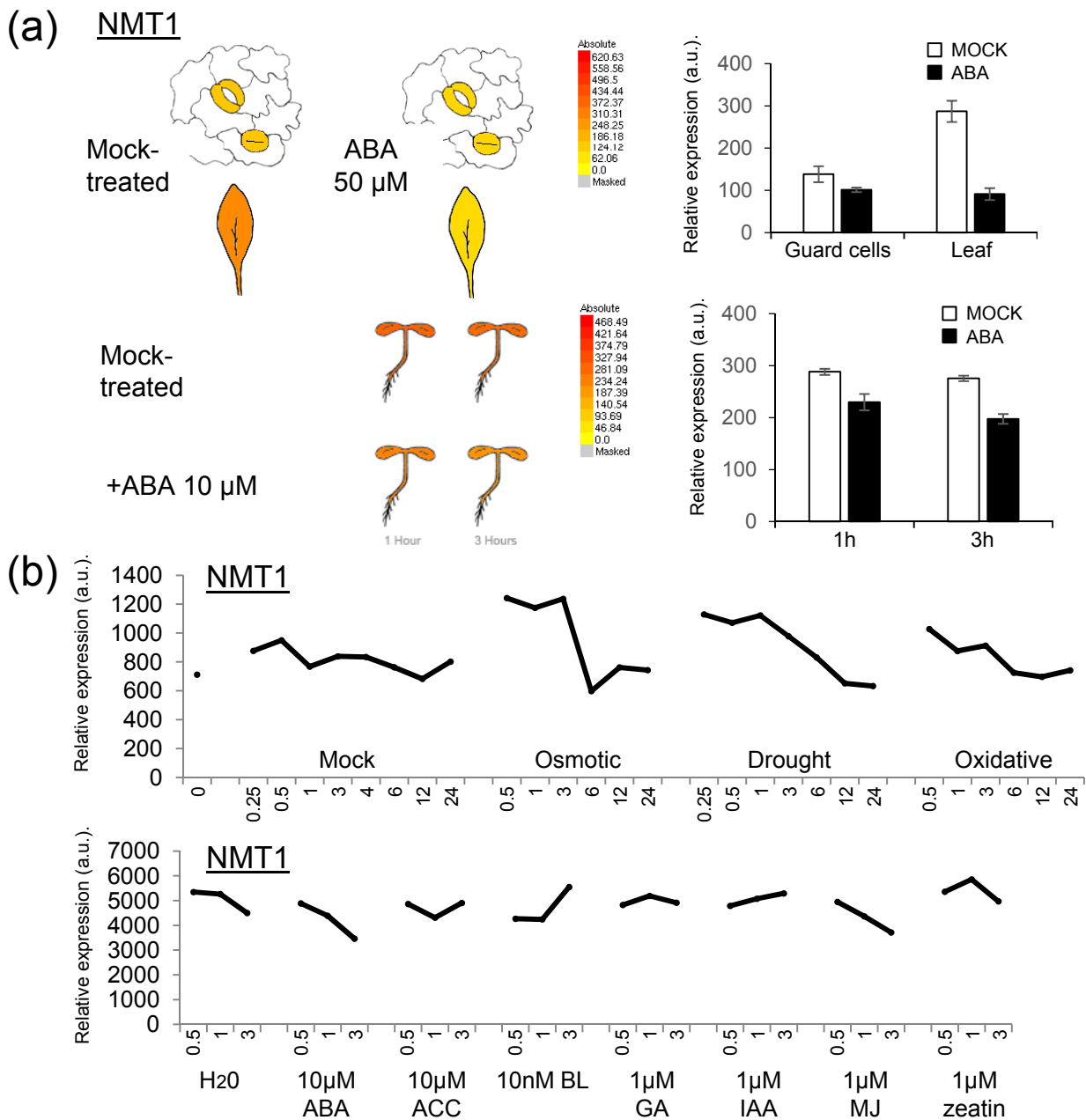


Figure S6. Expression of *NMT1* is down-regulated by ABA.

(a) Expression of *NMT1* in guard cells, leaves and seedlings that were mock- or 50 μM ABA-treated for 3h. Data were visualized using the eFP browser located in http://bar.utoronto.ca/efp_arabidopsis/cgi-bin/efpWeb.cgi (Winter et al., 2007). (b) Expression of *NMT1* in seedlings that were treated with different hormones (bottom) or submitted (top) to osmotic (300 mM mannitol), oxidative (10 μM methyl viologen) or drought (dry air stream until 10% loss of fresh weight) stress. Expression data were obtained from Affymetrix microarrays for *Arabidopsis* deposited in AtGenExpress public database (Goda et al., 2008) and visualized using the AtGenExpress Visualization tool located in <http://weigelworld.org/resources.html>.

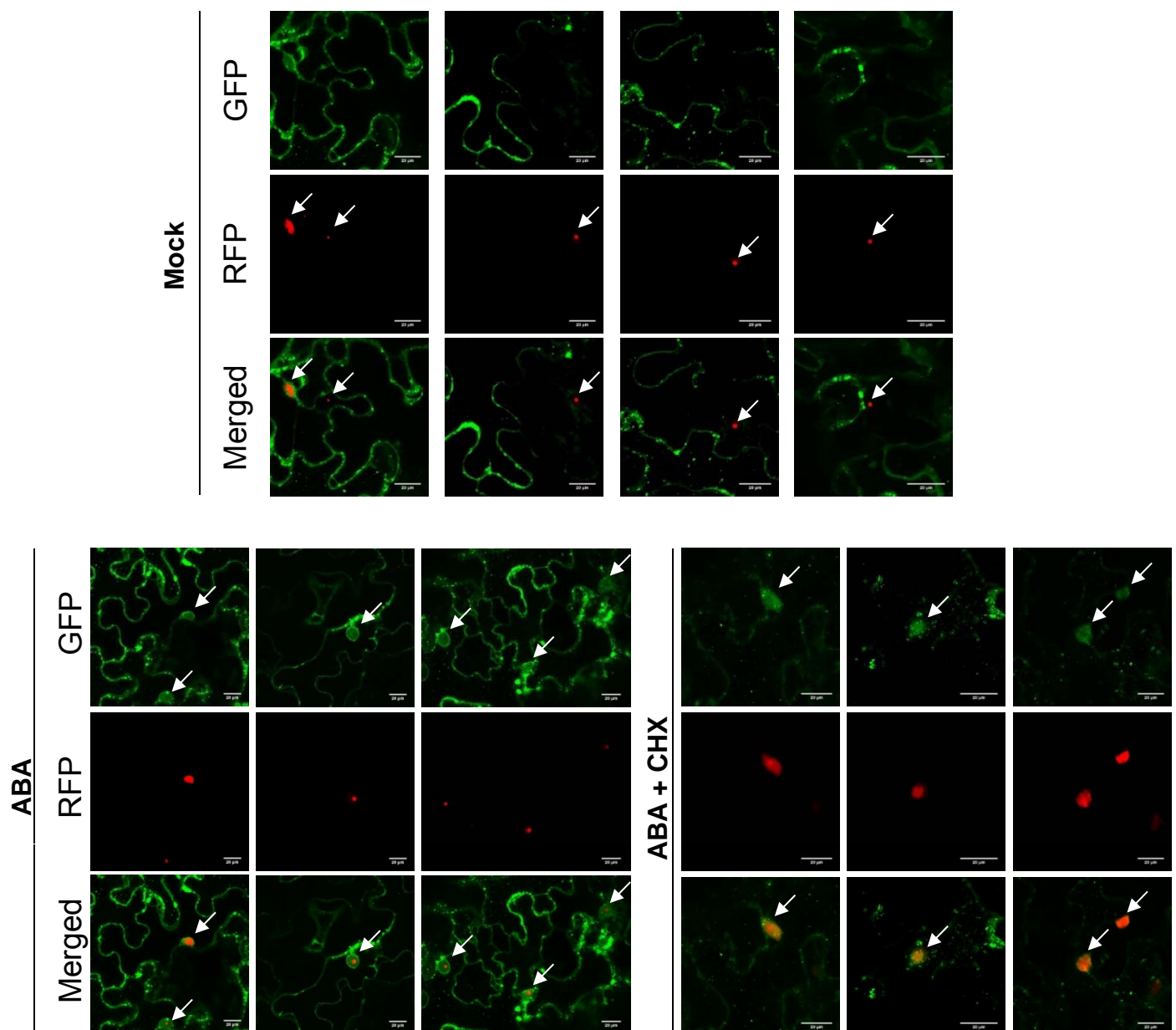


Figure S7. CHX treatment does not prevent ABA-induced shuttling of RGLG1 to cell nucleus in tobacco leaf cells.

The photographs show the subcellular localization of RGLG1-GFP expressed in agroinfiltrated epidermal leaf cells of *N. benthamiana* that were either mock-, 50 μM ABA-treated or simultaneously 50 μM ABA- and 100 μM CHX-treated for 6 h. Tobacco leaves were incubated with the indicated solutions at 72 h post-agroinfiltration. De novo biosynthesis of RGLG1 was inhibited by 100 μM CHX treatment. The GFP channel shows the subcellular localization of RGLG1-GFP, whereas the RFP channel shows the localization of the nucleolar marker Fib-RFP. CHX treatment led to simultaneous staining of nucleolus and nucleoplasm by Fib-RFP. Nuclei are indicated by arrows. Scale bars=20 μm .

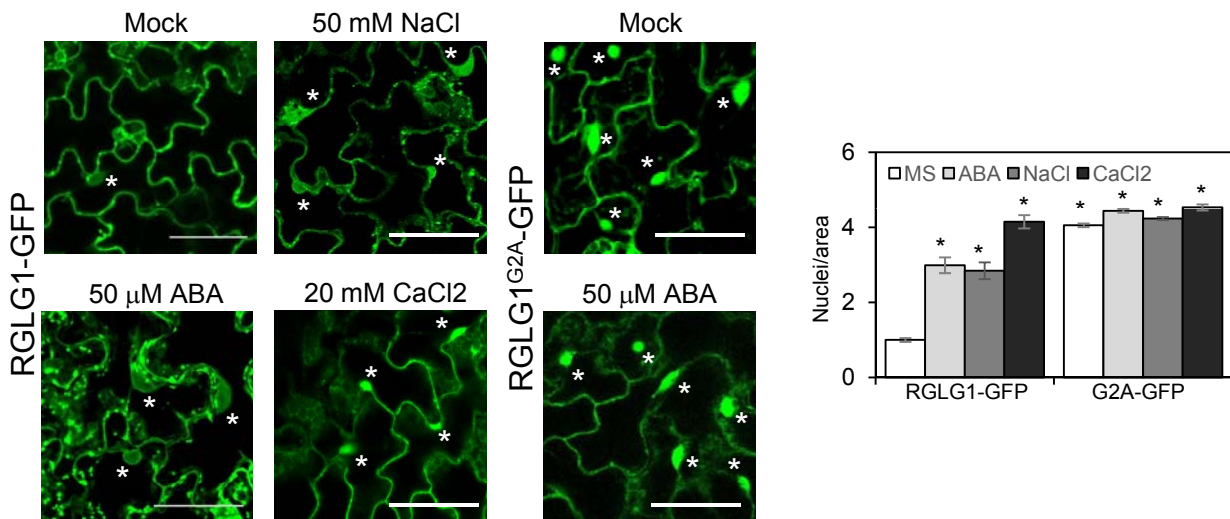


Figure S8. ABA, salt and calcium promote shuttling of RGLG1 to nucleus. Nuclear localization of RGLG1 was increased after 50 μM ABA, 50 mM NaCl or 20 mM CaCl₂-treatment for 6 h. RGLG1^{G2A}-GFP shows constitutive localization in nucleus. The photographs show the subcellular localization of RGLG1-GFP or RGLG1^{G2A}-GFP expressed in *Arabidopsis* transgenic lines using pMDC83. Nuclei are labeled with asterisks. Scale bars = 50 μm. Histograms indicate the relative number of nuclei decorated by RGLG1-GFP or RGLG1^{G2A}-GFP per area. Nuclei counting was done in sections of 40000 μm² (n=20 fields) from 5 independent plants, analyzed through a full z-series of confocal images. * indicates P < 0.05 (Student's t test) compared to the mock-treated sample of RGLG1-GFP.

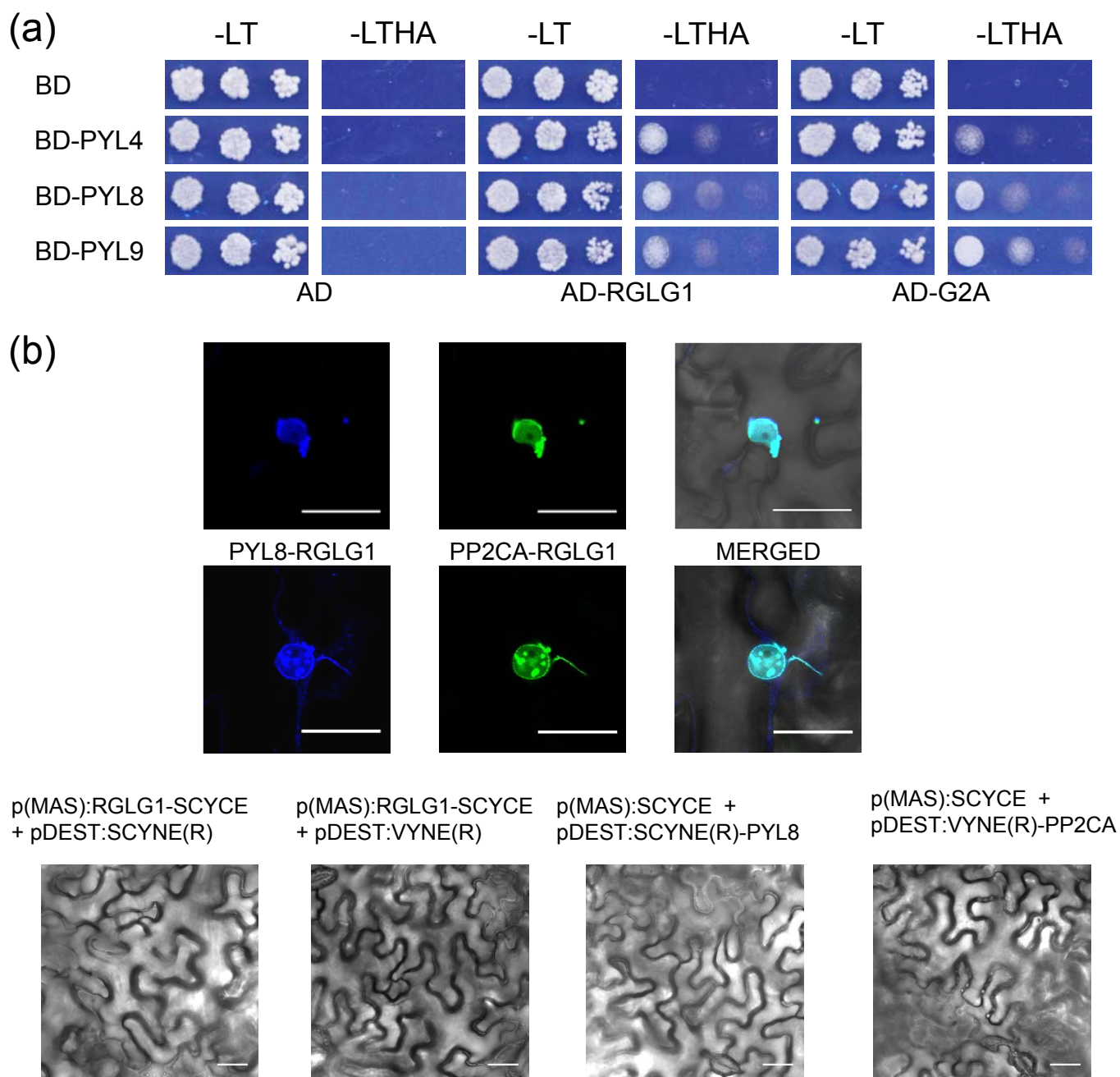


Figure S9. Interactions between RGLG1^{G2A} and PYLs in Y2H assay.

(a) Y2H interaction assay. Full-length PYLs were used as preys in pGBD vectors and wild-type RGLG1 or RGLG1^{G2A} as baits in pGAD vectors, respectively. Dilutions (10^{-1} , 10^{-2} , 10^{-3}) of saturated yeast cultures were spotted onto the plates and photographs were taken after 3 days. Yeast Nitrogen Base (YNB) medium -LT lacks Leu and Trp, whereas medium -LTHA lacks Leu, Trp, His and Ade. (b) Multicolor BiFC reveals the formation of PYL8-RGLG1-PP2CA complexes in the nucleus of tobacco leaves after ABA treatment. Confocal images of transiently transformed tobacco epidermal cells co-expressing SCFP^N-PYL8, RGLG1-SCFP^C and VENUS^N-PP2CA. The PYL8-RGLG1 interaction was visualized through reconstitution of the SCFP, whereas the RGLG1-PP2CA interaction gave rise to SCFP^C-VENUS^N fluorescent protein. To perform multicolor BiFC, RGLG1 was cloned into p(MAS)-SCYCE, PYL8 into pDEST-SCYNE(R) and PP2CA into pDEST-VYNE(R) vectors. The corresponding controls are included in the bottom panels. Constructs were delivered into tobacco leaves through *Agrobacterium*-mediated transfection. Leaves were examined using CLSM 48-72 h after infiltration and previous 50 μ M ABA-treatment for 1 h. Scale bars = 30 μ m.

Significance statement

Degradation of negative regulators is crucial for hormone signaling. ABA promotes the degradation of PP2CA through the RGLG1/5 E3 ligases and enhances the interaction of RGLG1/5 with PP2CA through an unknown mechanism. We show that ABA modifies the plasma membrane localization of RGLG1 by inhibiting its myristoylation and promoting cycloheximide-insensitive nuclear translocation, which allows interaction with nuclear PP2CA-receptor complexes. We explain how a hormone can modulate the interaction of an E3 ligase with its target.